Peer-reviewed version available at *Symmetry* **2020**, *12*, 177; doi:10.3390/sym12010177

*Article*

# Critically-finite dynamics on the icosahedron

**Scott Crass** [1]

[1] California State University, Long Beach; scrass@csulb.edu

**Abstract:** Drawing inspiration from a recent construction of a polyhedral structure associated with an icosahedrally-symmetric map on the Riemann sphere, the article shows how to build such "dynamical polyhedra" for other icosahedral maps. First, icosahedral algebra is used to determine a special family of maps with 60 periodic critical points. The topological behavior of each map is worked out and results in a geometric algorithm that constructs a system of edges—the dynamical polyhedron—in natural correspondence to a map's topology. It turns out that the maps' descriptions fall into classes the presentation of which concludes the paper.

**Keywords:** icosahedron, dynamics, equivariant

## 1. Overview

At the core of the quintic-solving algorithm devised by P. Doyle and C. McMullen is the dynamics of a special map with the symmetries of the icosahedron. [DM 1989] Their degree-11 map on the Riemann sphere has a critical set that coincides with the 20 vertices of the regular dodecahedron—a special icosahedral orbit. There is also a map of degree 19 under which the 12 icosahedral vertices are critical. A key property of these maps is a strong form of critical-finiteness: the critical points are periodic. Accordingly, their basins of attraction have full measure on the sphere. Moreover, each map gives rise to a forward invariant polyhedral structure of edges relative to which the map has an elegant geometric description. Due to the critical sets' achiral properties, the edges lie along great circles of reflective icosahedral symmetry. Indeed, the maps are also symmetric under reflection along the edges. Associated with the "11-map" is a dodecahedron and with the 19-map an icosahedron.

Recent work led to the discovery of two icosahedrally-symmetric maps with periodic critical sets of generic size, that is, 60-point orbits under the icosahedral group. [C 2014] The configurations of critical points take the form, in one case, of a soccer ball's vertices and, in the other, of the vertices on a type of dual soccer ball. In the case of a 60-point critical set, the question arises whether there are dynamically natural edges between the vertices. The previous effort constructed such a "dynamical polyhedron" for the soccer-ball map.

The current undertaking determines all icosahedral maps with internally periodic critical sets of size 60, where 'internal' means that the map permutes the critical points. We then study two special cases in some detail, describing the dynamical behavior in geometric terms. Subsequent discussion turns to edge-constructions for dynamical polyhedra. The critical sets, hence the systems of edges, for most of the maps form chiral configurations.

On terminology and graphics: "Facts" and graphical output are computational results generated by *Mathematica*. Notebooks that implement the computations are available at [C web].

## 2. Preliminaries: Icosahedral geometry, invariants, and equivariants

Since detailed descriptions of the geometric and algebraic structures associated with the icosahedron appear elsewhere ([K 1956], [DM 1989]), I will cite without explanation the ingredients required by the current investigation. For a brief summary of the relevant background, see [C 2014].

Peer-reviewed version available at Symmetry 2020, 12, 177; doi:10.3390/sym12010177



The orientation-preserving symmetries of the regular icosahedron form a group consisting of 60 rotations that act on the Riemann sphere $\mathbf{CP}^1$. The icosahedral group $\mathcal{I}$ is isomorphic to the alternating group $\mathcal{A}_5$. Furthermore, $\mathcal{I}$ can be extended by a reflection through a great circle to a group $\widetilde{\mathcal{I}}$ of 120 transformations half of which are orientation-reversing—that is, anti-holomorphic.

The ring of $\mathcal{I}$-invariant polynomials is generated by forms $F$, $H$, $T$ each of which vanishes on a special icosahedral orbit, that is, the vertices, face-centers, and edge-midpoints respectively. Accordingly, the generators have respective degrees 12, 20, 30 and satisfy a relation in degree 60.

Associated with an $\mathcal{I}$-invariant $G$ is an $\mathcal{I}$-equivariant rational map—$\mathcal{I}$-map for short—whose degree is one less than that of $G$. An *equivariant* is a map that commutes with the group action and thereby respects group orbits. Accordingly, an $\mathcal{I}$-map can be pushed down to a map on the quotient space $\mathbf{CP}^1/\mathcal{I}$. In the icosahedral case, maps of degree 11 and 19—$\phi$ and $\eta$ respectively—generate the module of $\mathcal{I}$-maps over the ring of $\mathcal{I}$-invariants.

## 3. Rational maps on $\mathbf{CP}^1$ as branched self-covers

A map $f : \mathbf{CP}^1 \to \mathbf{CP}^1$ with a forward invariant critical set $\mathcal{C}_f$ is a branched self-cover of $\mathbf{CP}^1$, meaning that, since $\mathcal{C}_f \subset f^{-1}(\mathcal{C}_f)$,

$$f : (\mathbf{CP}^1 - f^{-1}(\mathcal{C}_f)) \to (\mathbf{CP}^1 - \mathcal{C}_f)$$

is a covering map. A basic problem set by William Thurston is to determine a condition on a branched self-cover $f$ of $\mathbf{CP}^1$ that reveals whether or not $f$ is topologically conjugate to a rational map. Thurston formulated a negative result: a branched self-cover is not conjugate to a rational map when and only when a certain combinatorial obstruction exists. [DH 1993]

In recent work, Dylan Thurston discovered a positive characterization for rationality. [T 2016] Central to the theory is an *elastic graph spine* $G_f$ in $\mathbf{CP}^1 - \mathcal{C}_f$ the existence of which is necessary and sufficient for the self-cover to be conjugate to a rational map. (The full result applies to a class of maps that's larger than those with periodic critical points, but such maps are the focus here.) Put briefly, a "Thurston spine" is a graph 1) to which $\mathbf{CP}^1 - \mathcal{C}_f$ can be continuously deformed and 2) with a length function—giving rise to an elastic energy—defined on its edges such that when $f^{-1}$ is applied to the graph, the edges loosen in the sense of a decrease in elastic energy.

The cases of the 11-map, 19-map, and degree-31 soccer ball maps realize dynamical polyhedra with *complementary antipodal* behavior. That is, the sphere is carved into a cell-division with antipodal structure whose bounding edges form a graph $G$. Define a self-cover of $\mathbf{CP}^1$ by stretching a cell onto the complement of its antipodal cell. Up to homotopy, the resulting map $h$ is rational provided that it admits a Thurston spine. In private correspondence, Peter Doyle observes that the dual graph $\widehat{G}$ of $G$—essentially the dual polyhedron—gives such a spine. Backward iteration of $h$ relaxes the edges of $\widehat{G}$.

Drawing inspiration from these examples, we'll construct, for each map $f$ with 60 internally periodic critical points, an approximation to a graph in $\mathbf{CP}^1$ with dynamical integrity. Such a graph gives an $f$-invariant system of edges $\mathcal{E}_f$ that encloses faces with 2, 3, and 5-fold symmetry and whose vertices are the critical points. Since the maps are rational, they admit a Thurston spine. However, we can turn the discussion around and conjecture that, for each dynamical polyhedron of a 31-map with its topological description as a self-cover of the sphere, there is a natural Thurston spine. Note that, in the description of the self-covering behavior, a face $F$ maps to the complement of a cluster of faces that contains either $F$ or its antipodal face. Perhaps such a spine can be built by taking an $\mathcal{I}$-invariant graph that's dual to the polyhedral graph $\mathcal{E}_f$ and thereby encloses the critical points.

Peer-reviewed version available at Symmetry 2020, 12, 177; doi:10.3390/sym12010177



## 4. Icosahedral maps with periodic critical orbits

Our first task is to uncover each $\mathcal{I}$-map $f$ whose internally-periodic critical set $\mathcal{C}_f$ consists of a single $\mathcal{I}$-orbit of size 60. For such a *critically-finite* map, $\mathcal{C}_f$ is a superattracting set whose collective basins of attraction have full-measure on the sphere.

Maps with 60-point critical sets occur in degree 31 [C 2014] and the family of "31-maps" is given by

$$f_{(a,b)} = a\,H\,\phi + b\,F\,\eta.$$

To determine members of this family with periodic critical points, we follow a suggestion made by Peter Doyle and consider the maps induced on the quotient space $\mathcal{Q} = \mathbf{CP}^1/\mathcal{I}$. First note that the quotient map

$$q : \mathbf{CP}^1 \longrightarrow \mathcal{Q}$$

is realized, using homogeneous coordinates, by

$$(X, Y) = q(x, y) = (F(x, y)^5, H(x, y)^3).$$

Using an inhomogeneous parameter $Z = \frac{X}{Y}$, an $\mathcal{I}$-orbit is the collection of solutions $z$ to

$$Z = \frac{F(z)^5}{H(z)^3}.$$

Expressed diagrammatically (with the parameters suppressed):

$$\begin{array}{ccc} \mathbf{CP}^1 & \xrightarrow{\ f\ } & \mathbf{CP}^1 \\ {\scriptstyle q}\downarrow & & \downarrow{\scriptstyle q} \\ \mathcal{Q} & \xrightarrow{\ \widehat{f}\ } & \mathcal{Q} \end{array}$$

Letting $J_f$ be the jacobian matrix of $f$, the critical polynomial is $C_f = \det J_f$ and

$$\mathcal{C}_f = \{C_f = 0\}$$

is the critical set.

Invariant theory tells us that $C_f$ is $\mathcal{I}$-invariant and thus, expressible as a polynomial in $F$ and $H$. Note that we can dispense with the degree-30 invariant $T$ in light of the relation in degree 60 among $F^5$, $H^3$, and $T^2$. Since $C_f$ has degree-60, it can be expressed in terms of the quotient coordinates $X = F^5$ and $Y = H^3$.

**Fact 4.1.** *The critical polynomial of $f$ descends to $\mathcal{Q}$ as*

$$\widehat{C_f} = 4800\,b\,(12\,a + 19\,b)X - a\,(11\,a + 20\,b)Y.$$

Accordingly, $\widehat{\mathcal{C}_f} = \{\widehat{C_f} = 0\} \subset \mathcal{Q}$ has the parametrization

$$\Gamma = (a\,(11\,a + 20\,b), 4800\,b\,(12\,a + 19\,b)).$$

Now, we need to express the 31-maps $\widehat{f}$ on the quotient. First, note that composing an $\mathcal{I}$-invariant with an $\mathcal{I}$-map results in an $\mathcal{I}$-invariant. In the present context, we obtain

$$\widehat{f}(X, Y) = \widehat{f}(q(x, y)) = q(f(x, y)) = (F(f(x, y))^5, H(f(x, y))^3)\big|_{(F^5,H^3)\to(X,Y)}$$

Peer-reviewed version available at Symmetry 2020, 12, 177; doi:10.3390/sym12010177



where $F^5$ and $H^3$ are replaced by quotient coordinates $X$ and $Y$ after the $\mathcal{I}$-invariants $F(f(x,y))$ and $H(f(x,y))$ are expressed in terms of $F$ and $H$. Computation of the lengthy expressions for the components of $\widehat{f}$ can be found at [C web].

To determine 31-maps with periodic critical points, impose the condition that fixes the *point* $\widehat{\mathcal{C}_f}$ projectively in $\mathcal{Q}$; that is,

$$\widehat{f}(\Gamma) = \lambda\,\Gamma \quad \lambda \in \mathbf{C}.$$

Note the use of homogeneous parameters $(a,b)$ one of which is spent arranging for $\Gamma$ to be fixed. Furthermore, the fixed point condition in the quotient results in maps $f$ on $\mathbf{CP}^1$ for which the critical set is internally periodic—that is, fixed setwise. Accordingly, $\mathcal{C}_f$ decomposes into cycles the lengths of which are constrained by the action of $\mathcal{I}$.

**Proposition 4.2.** *Suppose that $v \in \mathbf{CP}^1$ is periodic under an $\mathcal{I}$-map $h$ and that $h(v) \in \mathcal{I}v$ (the orbit of $v$ under $\mathcal{I}$). The period of $v$ is either 2, 3, or 5.*

**Proof.** Let $p$ be the period of $v$ so that

$$v = h^p(v).$$

Furthermore, $h(v) = Av$ for some $A \in \mathcal{I}$. With $\alpha$ equal to the order of $A$, $\mathcal{I}$-equivariance of $h$ yields

$$h^2(v) = h(h(v)) = h(Av) = Ah(v) = A^2v.$$

Continuing inductively,

$$h^\alpha(v) = A^\alpha v = v$$

and the period of $v$ equals the order of $A$ which is 2, 3, or 5. □

Attention now turns to the equation $\widehat{f}(\Gamma) = \lambda\,\Gamma$ in $(a,b)$ whose solutions yield maps with 60 internally periodic critical points. This equation has the same solutions as one that's homogeneous in $(a,b)$, namely

$$R_\Gamma = \det\begin{pmatrix}\widehat{f}(\Gamma)\\ \Gamma\end{pmatrix} = 0.$$

**Fact 4.3.** *The polynomial $R_\Gamma$ factors as*

$$R_\Gamma = a^{13}\,b^{21}\,(3\,a+5\,b)^{31}\,P_3\cdot P_{12}\cdot P_{20}\cdot P_{24}$$

*where $P_k$ is a degree-k polynomial in a and b.*

**Fact 4.4.** *The three maps determined by the explicit factors involve a degeneracy to a lower degree map. For $3\,a+5\,b=0$, we get the identity $\epsilon$ boosted by the degree-30 invariant: $T\cdot\epsilon$. The cases where $a=0$ and $b=0$ produce boosted versions of the 11-map and 19-map: $H\cdot\phi$ and $F\cdot\eta$.*

Some intriguing numerology appears in the next factor.

**Fact 4.5.** *The three maps obtained by solving*

$$P_3 = (12\,a+19\,b)(11\,a+20\,b)(33\,a-95\,b) = 0$$

*possess critical points at the orbits of size 20, 12, 30 with respective multiplicities 3, 5, 2 and respective periods 1, 1, 2.*

These three maps deserve study; one issue is how the dynamics in the first two cases compares to that of $\phi$ and $\eta$, maps with the same periodic critical sets but different periods.

Peer-reviewed version available at Symmetry 2020, 12, 177; doi:10.3390/sym12010177



**Fact 4.6.** *The critical set for each map given by a root of*

$$\begin{aligned}P_{12} = {} & 262766592a^{12} - 5598533376a^{11}b - 110441517120a^{10}b^2 - 746454705120a^9b^3 \\ & - 2739682103040a^8b^4 - 6132369876696a^7b^5 - 8497318777952a^6b^6 - 6610001558770a^5b^7 \\ & - 1409601459875a^4b^8 + 2095583560000a^3b^9 + 1850218100000a^2b^{10} + 570668800000ab^{11} \\ & + 82308000000b^{12}\end{aligned}$$

*decomposes into* 30 *cycles of period two.*

**Fact 4.7.** *Twenty critical cycles of period-*3 *appear for each map whose parameter values are roots of*

$$\begin{aligned}P_{20} = {} & 9065321296035840a^{20} + 297447270441615360a^{19}b + 4657649128768576512a^{18}b^2 \\ & + 46235338429382479872a^{17}b^3 + 326041228341692697024a^{16}b^4 \\ & + 173477455084158094281 6a^{15}b^5 + 722084771695387155 6960a^{14}b^6 \\ & + 2405987287532594286 5304a^{13}b^7 + 6513136697106621843 0264a^{12}b^8 \\ & + 1445630108553472263919 98a^{11}b^9 + 2643656857858275391887 67a^{10}b^{10} \\ & + 3988151137431724960477 00a^9b^{11} + 4952415928188851051583 75a^8b^{12} \\ & + 5033223819926044822025 00a^7b^{13} + 4145038111170830727218 75a^6b^{14} \\ & + 2723474253989276249625 00a^5b^{15} + 1394385252901444825000 00a^4b^{16} \\ & + 5362688410681765000000 0a^3b^{17} + 1457947180182150000000 0a^2b^{18} \\ & + 2499250525650000000000ab^{19} + 2032382059200000000000b^{20}b^{12}.\end{aligned}$$

**Fact 4.8.** *For a map whose parameter values are roots of*

$$\begin{aligned}P_{24} = {} & 6683680085141304115 20a^{24} + 2696826938899486998 5280a^{23}b \\ & + 5169337619065618657443 84a^{22}b^2 + 6278245021807056570286080a^{21}b^3 \\ & + 5437907618017643326457 8560a^{20}b^4 + 3584257541006294306486476 80a^{19}b^5 \\ & + 1872659999168595359750108160a^{18}b^6 + 7972328332865032594746356736a^{17}b^7 \\ & + 2819377434723272788898380 0320a^{16}b^8 + 8395610437857871043290104 1920a^{15}b^9 \\ & + 2124832316869705447467786 26880a^{14}b^{10} + 4597952958598288383895397040 00a^{13}b^{11} \\ & + 8534519305171202074402296 11936a^{12}b^{12} + 1360052121063325875775069000720a^{11}b^{13} \\ & + 1858438540104362103609617554100a^{10}b^{14} + 2170118896655411970494805557500a^9b^{15} \\ & + 2153136983954016201268485528125a^8b^{16} + 1799688881704348373517523075000a^7b^{17} \\ & + 1251813375317007267354662750000a^6b^{18} + 7120539197083615793969200000000a^5b^{19} \\ & + 3229267865764403559395000000000a^4b^{20} + 1123702924627648450200000000000a^3b^{21} \\ & + 2818605436080499476000000000a^2b^{22} + 4537833560791747200000000000ab^{23} \\ & + 3521711632181760000000000000b^{24},\end{aligned}$$

*the critical set decomposes into* 12 *cycles of period five.*

In the period-2 cases, the critical sets exhibit both achiral and chiral structures. For maps with critical cycles of length three or five, the configurations of critical points are chiral.

## 5. Periodic cycles

We begin by determining which cycles occur. The proof of Proposition 4.2 indicates that, when an $\mathcal{I}$-map $f$ satisfies $f(x) = Ax$ for some $A \in \mathcal{I}$, the cyclic orbits of $x$ under $f$ and $A$ coincide. Although

Peer-reviewed version available at Symmetry 2020, 12, 177; doi:10.3390/sym12010177



the critical sets for the maps are disjoint, most of them take on a “rhombicosidodecahedral" pattern that consists of 30 quadrilaterals, 20 triangles, and 12 pentagons. We’ll refer to such a structure as $B_{62}$. There are five exceptions: the two soccer ball maps and the above-mentioned maps whose critical sets degenerate into 12 pentagonal centers, 20 triangular centers, and 30 quadrilateral centers.

First, consider a “schematic" $B_{62}$ as a configuration of 60 vertices and one of the 15 order-2 axes $a_2$ through a pair of antipodal quadrilaterals. The stabilizer of $a_2$ in $\mathcal{I}$ is the dihedral group $D_2$ under which the $B_{62}$ vertices decompose into fifteen sets of four points. The schematic $B_{62}$ appears in Figure 1 and, with $a_2$ at the center, indicates pairings specified by the $D_2$ action. Of course, for each label, another pair occurs on the hidden hemisphere. There are twelve non-antipodal pairs each of which corresponds to a root of $P_{12}$ and thereby to a 31-map. For example, the map corresponding to the four points (two are hidden from view) labeled 1 exchanges the pair on the near side as well as the pair on the far side. The map has the same effect on the other quadruples of vertices that are in the $\mathcal{I}$-orbit of the quadruple labeled 1.

As for the eight points labeled 13, they appear in antipodal pairs and can be associated with three maps: the special map with doubly-critical behavior at the 30-point orbit and the two soccer ball maps. Under a map associated with label 13, the image of a critical point is its antipode. Accordingly, the critical sets of these maps have achiral arrangements.

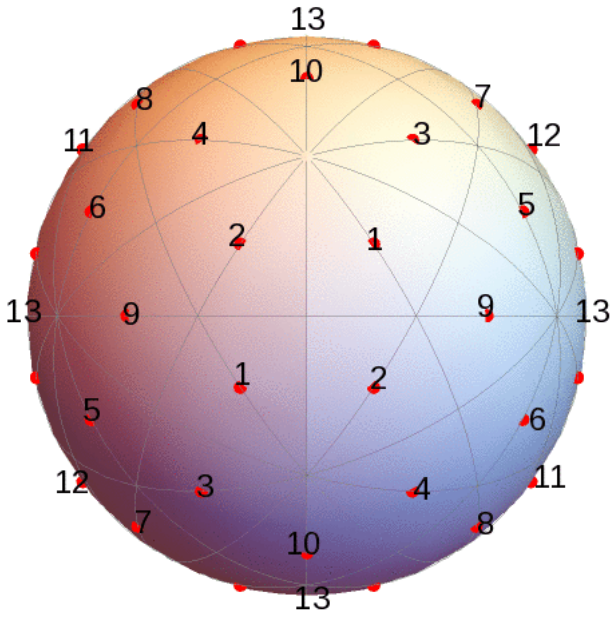


**Figure 1.** Schematic $B_{62}$ labeled for period-2 behavior

Similar considerations hold in the cases of 3-fold and 5-fold axes where the stabilizing subgroups are $D_3$ and $D_5$. Respectively, the actions of the stabilizers decompose $B_{62}$ vertices into orbits of size six and ten. These dihedral orbits appear as ten pairs of triples and six pairs of quintuples. For each of the two 3-cycles that a pair of triples can undergo, there’s a map given by a root of $P_{20}$ that cycles the triple in the prescribed way—as well as each triple in its $\mathcal{I}$-orbit. This behavior accounts for all 20 of the maps obtained from the roots of $P_{20}$. In the case of a 5-fold axis $a_5$, each pair of quintuples can undergo four 5-cycles. Since there are six such quintuple pairs associated with $a_5$, we count a total of 24 distinct 5-cycles of $B_{62}$ vertices, one for each root of $P_{24}$. So, for a 31-map obtained from a $P_{24}$ root, each $B_{62}$ vertex undergoes an $\mathcal{I}$-equivalent 5-cycle.

Peer-reviewed version available at Symmetry 2020, 12, 177; doi:10.3390/sym12010177



When a $B_{62}$ configuration is chiral—as in most of the period-2 and all of the period-3 and period-5 cases, each map $f(z)$ has a partner $\overline{f}(z) = \overline{f(\overline{z})}$, obtained by conjugating the coefficients. In geometric terms, the critical configurations for $f$ and $\overline{f}$ are mirror images across a great circle of icosahedral symmetry so that if the triples or quintuples of critical points for $f$ undergo a cycle in one orientation, the triples or quintuples for $\overline{f}$ are cycled in the opposite orientation, thereby producing distinct and inverse permutations as seen on a schematic polyhedron.

## 6. Special behavior on a fundamental domain

Our ultimate goal is to manufacture polyhedral structures that are naturally associated with critically-finite 31-maps. Before taking up that issue, let's consider the elegant behavior of two such maps when restricted to a fundamental domain under the extended icosahedral group $\widetilde{\mathcal{I}}$. Strictly speaking, the collection of fundamental domains provides a polyhedral structure, but only for achiral maps. Subsequent constructions will be based specifically on the configuration of critical points.

Figure 2 displays critical configurations for two maps $g$ and $h$; note that each set is achiral and takes on a $B_{62}$ structure. Recall that the critical points have period two. In homogeneous coordinates, $g$'s numerical form is approximately

$$\begin{aligned} g \approx (&-x(x^{30} - 867.9384578x^{25}y^5 - 7698.743615x^{20}y^{10} + 17873.48698x^{15}y^{15} \\ &- 19927.97155x^{10}y^{20} - 449.0553201x^5y^{25} + 7.069095750y^{30}), \\ &- 7.069095750(x^{30}y + 63.52372862x^{25}y^6 - 2819.026967x^{20}y^{11} - 2528.397919x^{15}y^{16} \\ &- 1089.070496x^{10}y^{21} + 122.7792759x^5y^{26} + 0.1414608085y^{31})). \end{aligned}$$

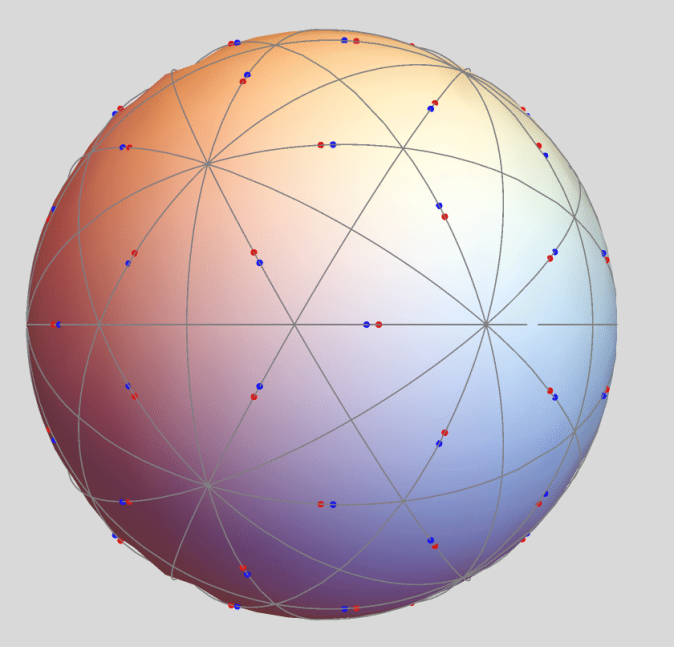

**Figure 2.** Achiral critical sets of $g$ (red) and $h$ (blue)

The achirality of $g$ and $h$ results from the fact that $\overline{g} = g$ and $\overline{h} = h$. As a result, the maps are equivariant under reflection through the real axis (that is, complex conjugation) as well as under reflection through each of the fourteen other great circles that form the icosahedral system of 120 triangles on the sphere—called "235 triangles" due to the order of the action that stabilizes a vertex. Accordingly, we can take a 235 triangle $X$ for a fundamental domain of $\widetilde{\mathcal{I}}$. (Illustrated in Figures 3 and 4).

Peer-reviewed version available at Symmetry 2020, 12, 177; doi:10.3390/sym12010177



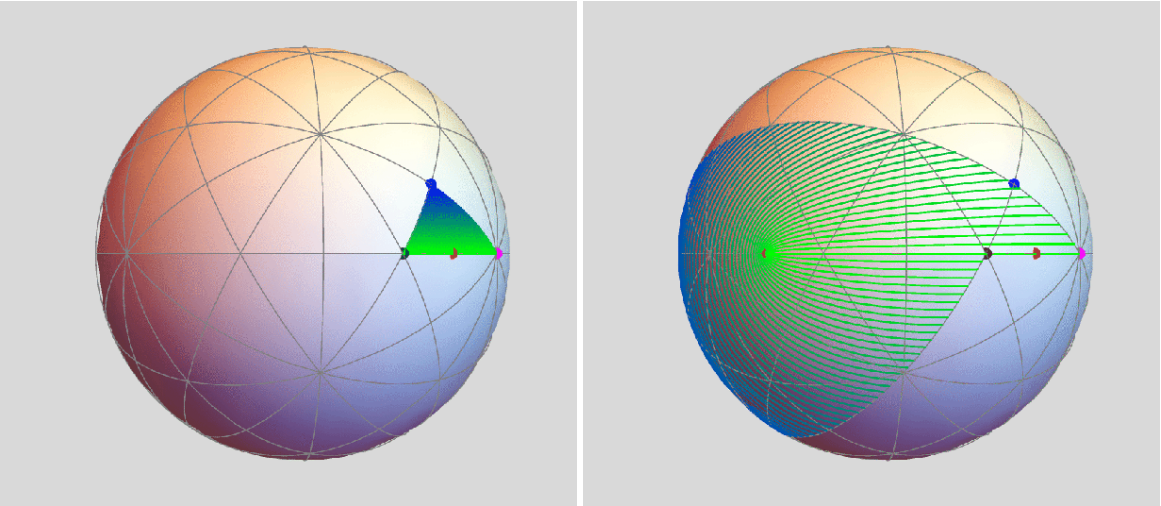

**Figure 3.** Fundamental triangle and its image under $g$

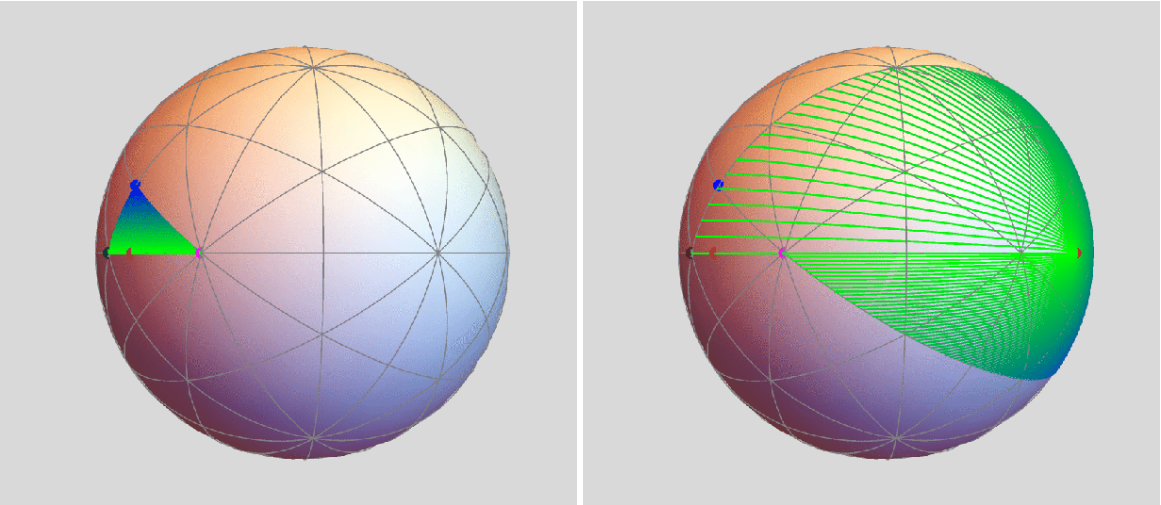

**Figure 4.** Fundamental triangle and its image under $h$

Because the great circles of reflective symmetry are pointwise fixed by a reflection in $\widetilde{\mathcal{I}}$, general equivariant theory requires that an achiral $\widetilde{\mathcal{I}}$-map preserves such a circle setwise. It follows that the image of a fundamental triangle $X$ is the union of such triangles. In fact, the plot reveals that $g(X) = X \cup L_g$ where $L_g$ is the lune formed by extending the sides of $X$ that form its right angle. Beginning at the 2-fold vertex $p$, extend one edge away from the 5-fold vertex and extend the other edge toward the 3-fold vertex. Continue the extensions along the respective great circles until they meet at the antipode of $p$.

Referring to the image on the left in Figure 3, $X$ is approximately foliated by line segments parallel to its hypotenuse—the segment color varies from green to blue. The distinguished point on the interior of the hypotenuse is critical. On the right we see the images of the foliating segments. The bending and attracting behavior that occurs at the critical point's image illustrates the branching that occurs at the critical value. Since $L_g$ is one-quarter of the sphere, it encloses 30 fundamental triangles. Hence, $g$ maps $X$ to 31 fundamental triangles, a topological manifestation of $g$'s degree.

An exactly analogous description applies to $h$, depicted in Figure 4. In this case, $h(X) = X \cup L_h$ and the lune $L_h$ forms by extending the respective perpendicular sides of $X$ from the 2-fold vertex away from the 3-fold vertex and toward the 5-fold vertex.

Peer-reviewed version available at Symmetry 2020, 12, 177; doi:10.3390/sym12010177



## 7. Dynamical polyhedra

Realizing the structure of a spherical polyhedron requires a system of edges between critical points that appears naturally from a map's behavior. Serving as an archetype is the soccer ball map where the collection of edges is a forward invariant set in which the image of a single face $K$ is a union of faces that are canonically associated with $K$.

### *7.1. Constructing edges*

What follows is a fairly elaborate description of a method that, for a 31-map $f$, constructs edges between *adjacent* vertices (periodic critical points). Working on the sphere, adjacency is determined by triangular and pentagonal arrangements of critical points nearest to 3-fold and 5-fold axes. In every case, a common heuristic element first connects adjacent vertices by a great-circle arc. Given such a *proto-edge* $T_0$ or $P_0$ (depending upon whether the arc spans adjacent triangular vertices $(t_1, t_2)$ or pentagonal vertices $(p_1, p_2)$, we use the image $f(T_0)$ or $f(P_0)$ to indicate a collection of edges to which an *actual* edge maps. To be specific, say that we're approximating a pentagonal edge $P$ that spans $(p_1,p_2)$—illustrated in Figure 5. The procedure generates the actual edge as a result of an infinite number of iterative steps.

The first step identifies an ordered set of $B_{62}$ vertices

$$(v_0 = f(p_1), \ \dots \ , v_k, \ \dots \ , v_m = f(p_2))$$

through which $f(P)$ is to pass. Given an adjacent pair of triangular vertices $(v_{k-1}, v_k)$, there's a unique element $S_k \in \mathcal{I}$ such that either

$$(S_k(t_1), S_k(t_2)) = (v_{k-1}, v_k) \quad \text{or} \quad (S_k(t_2), S_k(t_1)) = (v_{k-1}, v_k).$$

Similarly, if $(v_{k-1}, v_k)$ is an adjacent pair of pentagonal vertices, a unique $S_k \in \mathcal{I}$ satisfies either

$$(S_k(p_1), S_k(p_2)) = (v_{k-1}, v_k) \quad \text{or} \quad (S_k(p_2), S_k(p_1)) = (v_{k-1}, v_k).$$

Connect $(v_{k-1}, v_k)$ by the appropriate "pushed" proto-edge $Q_0^k = S_k(X_k)$ where $X_k$ is either $P_0$ or $T_0$. Every $(v_{k-1}, v_k)$ in $(v_0, \dots, v_m)$ is now spanned by great circle arcs.

In order to approximate a triangular edge $T$, the technique gives pushed edges

$$(U_0^1 = Z_1(Y_1), \ \dots \ , U_0^n = Z_n(Y_n))$$

where $Z_k \in \mathcal{I}$ is the analogue of $S_k$ and $Y_k$ is either $P_0$ or $T_0$. Comparing the pushed paths $(Q_0^1, \dots, Q_0^m)$ and $(U_0^1, \dots, U_0^n)$ to the respective images $f(P_0)$ and $f(T_0)$ reveals their homotopic equivalence, as Figure 5 illustrates in the plane.

Peer-reviewed version available at Symmetry 2020, 12, 177; doi:10.3390/sym12010177



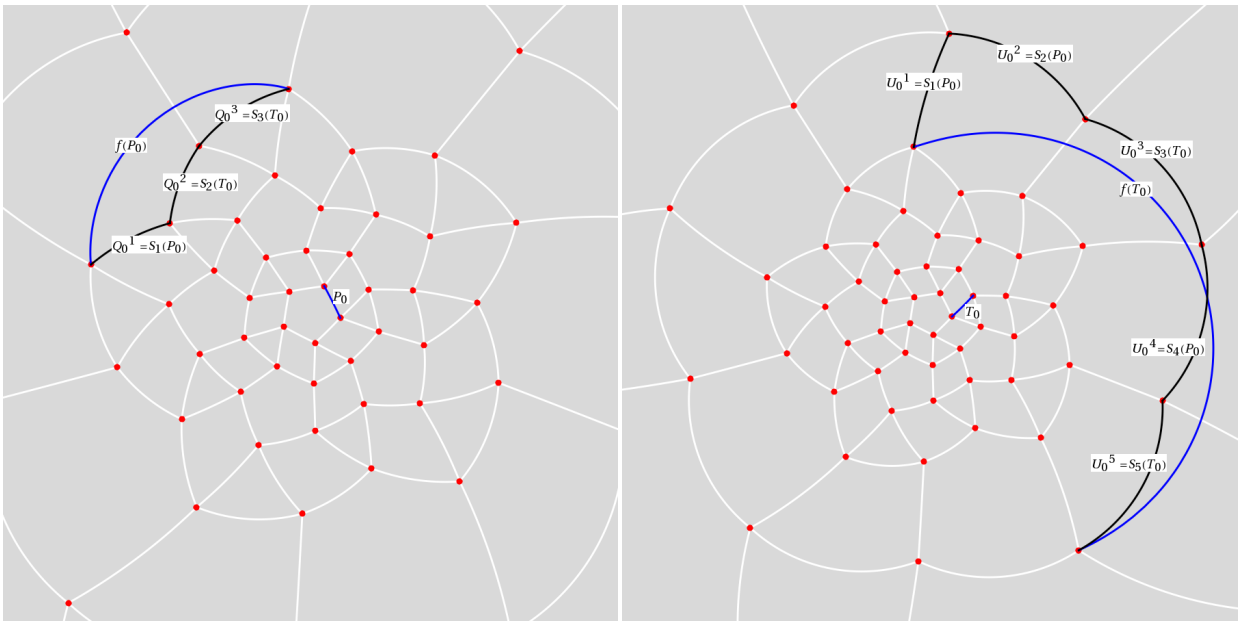


**Figure 5.** Homotopy between select proto-edges and the image of a proto-edge for a pentagon in a $B_{62}$ under one of the 31-maps $f$. The images of the proto-edges $P_0$ and $T_0$ (blue arcs) are respectively homotopic to a chain of pushed versions of $P_0$ and $T_0$ (black arcs). In this sample, the pushed edges associated with $f(P_0)$ are PPT (pentagon-pentagon-triangle) while those associated with $f(T_0)$ are PPTPT.

Peer-reviewed version available at Symmetry 2020, 12, 177; doi:10.3390/sym12010177



There's a degree of freedom in choosing the endpoints of the $Q_0^k$ and $U_0^k$. Here, we select endpoints so that a map's geometric description respects "$P$-caps"—a pentagonal face with its surrounding five triangles and five quadrilaterals. Figure 6 shows a schematic $P$-cap in a planar $B_{62}$ structure.

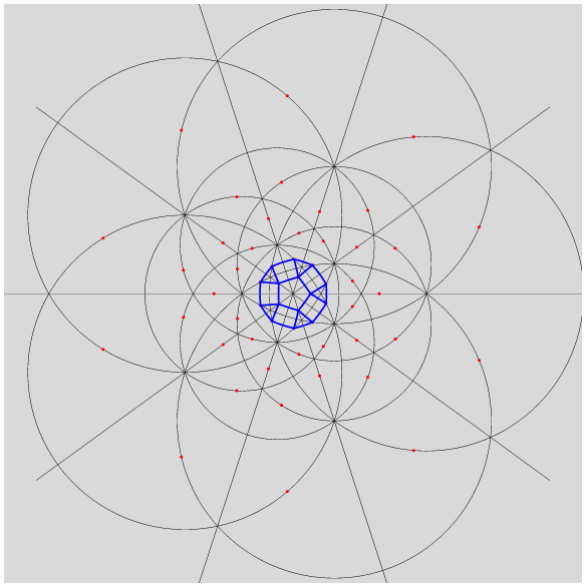

**Figure 6.** A $P$-cap in a $B_{62}$

In step two we use suitable branches of $f^{-1}$ to pull back the segments $(Q_0^1, \ldots, Q_0^m)$ to a first generation edge $P_1$ between $(p_1, p_2)$. In practice, this is accomplished as follows.

1. Select equally-spaced points $(b_k^1, \ldots, b_k^{n_k})$ along each $Q_0^k$.
2. Compute the elements in $f^{-1}(b_k^\ell)$ for $\ell = 1 \ldots n_k$.
3. Extract from $f^{-1}(b_k^\ell)$ the inverse image points $(a_k^1, \ldots, a_k^{n_k})$ that minimize the sum of the distances to $p_1$ and $p_2$.
4. Taylor expand $f$ about $(a_k^1, \ldots, a_k^{n_k})$.
5. Obtain the desired single-valued branch $\gamma_k^\ell$ of $f^{-1}$ by inverting the Taylor series for $f$ at $a_k^\ell$. The choice of branch yields
$$\gamma_k^\ell(b_k^\ell) = a_k^\ell.$$
6. Compute the "pulled" segmented paths that span $(p_1, p_2)$:
$$\begin{aligned} P_1^1 &= (\gamma_1^1(Q_0^1), \ \ldots \ , \gamma_1^{n_1}(Q_0^1)) \\ &\vdots \\ P_1^m &= (\gamma_m^1(Q_0^m), \ \ldots \ , \gamma_m^{n_m}(Q_0^m)). \end{aligned}$$

Notice that, in a pulled segment, different branches of the inverse map are applied to the *same* parametrized segment $Q_0^k$. We arrive at the appropriate pulled segment by selecting a subinterval of the parameter interval. In the triangular case, we get first-generation pulled edges $(T_1^1, \ldots, T_1^n)$.

Step three begins an iteration of the process by moving the pulled segments to the pushed locations:

$$(Q_1^{1,1} = S_1(X_1^1), \ \ldots \ , Q_1^{m,m} = S_m(X_1^m)) \quad \text{and} \quad (U_1^{1,1} = Z_1(Y_1^1), \ \ldots \ , U_1^{n,n} = Z_n(Y_1^n))$$

where $X_1^k$ and $Y_1^k$ are either $P_1^k$ or $T_1^k$. Observe that the subscript of $P$, $Q$, $T$, and $U$ is the generation number. The group elements $S_k$ and $Z_k$ act on each component of the respective $X_1^k$ or $Y_1^k$. For example,

$$Q_1^{k,\ell} = S_k(P_1^\ell) = \ (S_k(\gamma_k^1(Q_0^\ell)), \ \ldots \ , S_k(\gamma_k^{n_k}(Q_0^\ell))).$$

Peer-reviewed version available at Symmetry 2020, 12, 177; doi:10.3390/sym12010177



Applying the push transformations $S_k$ to the centers of Taylor expansion $a_\ell^r$ produces a fresh set of points

$$(b_k^{\ell,1} = S_k(a_\ell^1), \ \dots \ , b_k^{\ell,n_k} = S_k(a_\ell^{n_k}))$$

on the pushed segments $Q_1^{k,\ell}$. Inverse images of the $b_k^{\ell,i}$ then become a new set of Taylor centers $a_k^{\ell,i}$ with associated branches $\gamma_k^{\ell,i}$ of $f^{-1}$.

Next, the fourth step constructs second-generation segments at $(p_1, p_2)$ and $(t_1, t_2)$ by pulling back the pushed edges. For a pentagonal edge,

$$P_2^{k,\ell} = (\gamma_k^{\ell,1}(Q_1^{k,\ell}), \ \dots \ , \gamma_k^{\ell,n_k}(Q_1^{k,\ell})).$$

The second-generation approximation of $P$ is the collection of segments

$$((P_2^{1,1}, \ \dots \ , P_2^{1,n_1}), \ \dots \ , (P_2^{m,1}, \ \dots \ , P_2^{m,n_m})).$$

As before, when the second-generation segments are pushed and then pulled, the group elements as well as the branches of $f^{-1}$ distribute over components.

Letting the number of iterations of the push-pull algorithm grow without bound, the edge $P$ emerges:

$$\bigcup_{(k_i)} \cdots \circ (\gamma_{k_{r+1}}^{k_r,\dots,k_1} \circ S_{k_{r+1}}) \circ (\gamma_{k_r}^{k_{r-1},\dots,k_1} \circ S_{k_r}) \circ \cdots \circ (\gamma_{k_2}^{k_1} \circ S_{k_2})(P_0) = P$$

where $(k_i)$ ranges over all permissible sequences. Grouping the push-pull action as $(\gamma \circ S)$ produces a set that spans the endpoints of $P_0$. A similar dynamic yields a triangular edge $T$.

Evidently, for a selected $(k_i)$, the procedure converges due to the collection $\{\gamma_{k_r}^{k_{r-1},\dots,k_1} \circ S_{k_r}\}$ being a normal family. ([B 1991], Theorem 9.2.1) In more geometric terms, under $f$ a proto-edge undergoes a net expansion. As exemplified in Figure 5, $P_0$ experiences roughly a three-fold stretch and $T_0$ expands approximately by a factor of five. The expanding behavior occurs on the complement of a neighborhood of the superattracting periodic points. When pulled back, the pieces of the pushed proto-edges that are bounded away from the critical points undergo a net contraction reciprocal to the expansion under forward iteration. In each push-pull cycle, this contraction occurs away from points in the pre-critical set while the push transformation is an spherical isometry. The result is clustering among the pulled-back points.

With $P$ and $T$ in hand, the icosahedral action produces a system of edges for a dynamical polyhedron: $\mathcal{E}_f = \mathcal{I}(P) \cup \mathcal{I}(T)$. Graphical constructions of second-generation approximations for the 31-maps appear in the following section.

**Proposition 7.1.** *The system of edges $\mathcal{E}_f$ is forward invariant under $f$.*

**Proof.** The push-pull construction of $P$ iterates the map $\gamma \circ S$ where, for ease of description, indices are suppressed. That is,

$$(\gamma \circ S)^r(P_0) \xrightarrow{r\to\infty} A \subset P.$$

(Since the $\gamma$ maps are local inverses of $f$, the limit set $A$ is only contained in $P$.) Applying $f$ gives

$$\begin{aligned}
&f \circ (\gamma \circ S)^r(P_0) \xrightarrow{r\to\infty} f(A)\\
&f \circ (\gamma \circ S) \circ (\gamma \circ S)^{r-1}(P_0) \xrightarrow{r\to\infty} f(A)\\
&(f \circ \gamma) \circ S \circ (\gamma \circ S)^{r-1}(P_0) \xrightarrow{r\to\infty} f(A)\\
&S \circ (\gamma \circ S)^{r-1}(P_0) \xrightarrow{r\to\infty} f(A).
\end{aligned}$$

Peer-reviewed version available at Symmetry 2020, 12, 177; doi:10.3390/sym12010177



Since

$$S \circ (\gamma \circ S)^{r-1}(P_0) \xrightarrow{r\to\infty} S(A),$$

$f(A) = S(A) \subset \mathcal{I}(P)$. Of course, a similar result holds for a triangular edge $T$. □

*7.2. Combinatorial classification*

Here, we'll treat the behavior of the 56 maps that result from solving the parameter equations $P_{12} = 0$, $P_{20} = 0$, and $P_{24} = 0$. For a map $f$, the computational graphics displayed in Section 8 solves a combinatorial problem: Given a face $A$ of $f$'s polyhedron, what collection of faces does $f(A)$ cover?

Referring to the graphical results, the second-generation system of edges $\mathcal{E}_f$ appears in white. (Note the change in usage: here, $\mathcal{E}_f$ refers to an approximation of the actual system of edges.) Gaps around the critical points are due to the large expansion under the pullback. Given a point $z_0$ on an edge, we pullback to $f^{-1}(z_0)$ by solving $f(z) = z_0$. In the plot on the left side, the gray curves correspond to the inverse image $f^{-1}(\mathcal{E}_f)$. The pulled-back edges reveal the beginnings of a fractal structure: within each face $A$ there is a collection of "pre-faces" that indicates what face-types $f(A)$ covers. Note that $\mathcal{E}_f$ is close to being a subset of $f^{-1}(\mathcal{E}_f)$—visual evidence that $\mathcal{E}_f$ is approximately $f$-invariant.

Using a map-coloring procedure, we can discern which faces $f(A)$ covers. Given a map $f(z)$ on $\mathbf{C}$, define color functions for hue and luminosity

$$H_f(z) = \frac{\text{Arg}(f(z))}{2\,\pi} \quad \text{and} \quad L_f(z) = 2^{-|f(z)|}$$

where Arg $\in [0, 2\,\pi]$ is a branch of the argument taken modulo $2\,\pi$. Each function takes on values in $[0, 1]$ with hue varying from blue to green and luminosity from bright to dark.

The plots on the right show $\mathcal{E}_f$ overlaid on a reference coloring for the identity map $I$. On the left we see the pulled-back faces on top of the coloring for a 31-map $f$. By matching the color properties of a pre-face on the left with those of a face on the right, we can determine which face turns out to be its image. That is, $f(z) = w$ when

$$(H_f(z), L_f(z)) = (H_I(w), L_I(w)).$$

For instance, the point at infinity is the center of a pentagonal face $P_\infty$. As a consequence, dark pentagonal pre-faces cover $P_\infty$.

The maps are classified according to their combinatorial and topological descriptions. Pullback structures within a class are topologically equivalent.

By way of illustrating the combinatorics and topology, we consider the map $g$ introduced previously. Its critical set realizes an achiral $B_{62}$ configuration whereby the critical points lie on the mirrors of reflective icosahedral symmetry. As is the case for all of the 31-maps, the centers of a pentagon and triangle are fixed by $g$ while a quadrilateral's center is sent to its antipode.

The geometric behavior of $g$ differs from that of the two soccer ball maps—which are not included here since their dynamical polyhedra do not have $B_{62}$ structure and they have been considered elsewhere. A face does not map to the complement of an antipodal face, as that would require the degree to be 61. Computational graphics (plots at the top of Class I) reveals that $g$ wraps a face onto a union of $P$-caps that is icosahedrally associated with the face. The image of a pentagonal face $P$ covers the cap to which it belongs as well as the five caps that intersect $P$'s cap. For a triangular face $T$, $g(T)$ covers the three caps whose intersection includes $T$. Finally, the image of a quadrilateral $Q$ covers the complement of four $P$-caps two of which intersect $Q$ while the other two caps intersect the former two caps.

Using its geometric description, we can work out $g$'s topological degree by counting inverse images. The relevant data are recorded in Table 1 as the number of faces of each type that belong to the

Peer-reviewed version available at Symmetry 2020, 12, 177; doi:10.3390/sym12010177



$g$-image of a given face-type. For instance, the first row reports that a pentagon maps to six caps the union of which contains six pentagons, fifteen triangles, and twenty quadrilaterals.

| | | $P$ | $T$ | $Q$ |
|---|---|---|---|---|
| $P$ | $\longrightarrow$ | 6 | 15 | 20 |
| $T$ | $\longrightarrow$ | 3 | 10 | 12 |
| $Q$ | $\longrightarrow$ | 8 | 8 | 15 |

**Table 1.** Images of faces under $g$

The number of times a pentagonal face is covered equals the total number of pentagons that appear as images of faces divided by the number of pentagonal faces. Reading down the $P$ column,

$$\frac{12 \cdot 6 + 20 \cdot 3 + 30 \cdot 8}{12} = 31.$$

Similar treatment of triangular and quadrilateral faces yields the number of faces in the inverse image of the respective face:

$$\frac{12 \cdot 15 + 20 \cdot 10 + 30 \cdot 8}{20} = \frac{12 \cdot 20 + 20 \cdot 12 + 30 \cdot 15}{30} = 31.$$

The gallery of plots places the maps into combinatorial classes, with three exceptions. Each class has a complementary class for which the topological description replaces "$n$ $P$-caps about $X$" by "complement of $n$ $P$-caps about $\widetilde{X}$" and "complement of $n$ $P$-caps about $X$" by "$n$ $P$-caps about $\widetilde{X}$" where $\widetilde{X}$ is the antipode of $X$. Of course, a chiral map $f$ and its heterochiral partner $\overline{f}$ (not shown) belong to the same class.

## 8. Periodic table

Class I

$P \longrightarrow$ six $P$-caps about $P$
$T \longrightarrow$ three $P$-caps about $T$
$Q \longrightarrow$ complement of four $P$-caps about $Q$

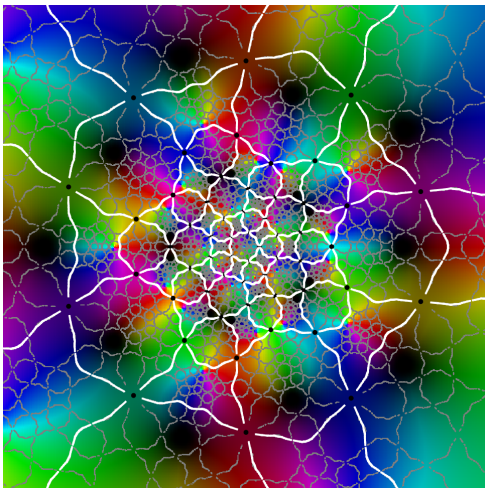

the map $g$ discussed in Section 6

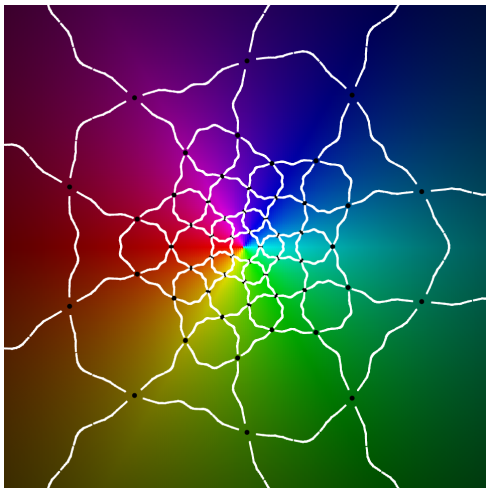

period 2, achiral

Peer-reviewed version available at *Symmetry* **2020**, *12*, 177; doi:10.3390/sym12010177



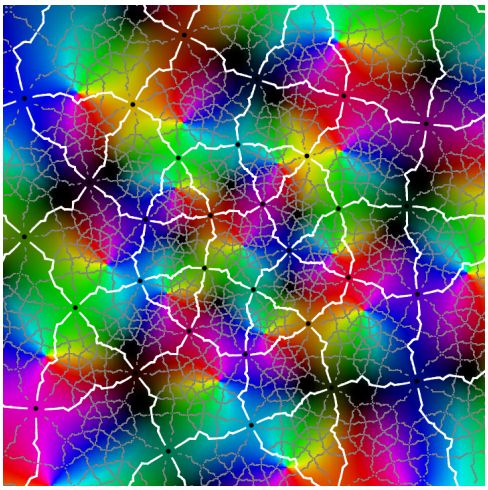

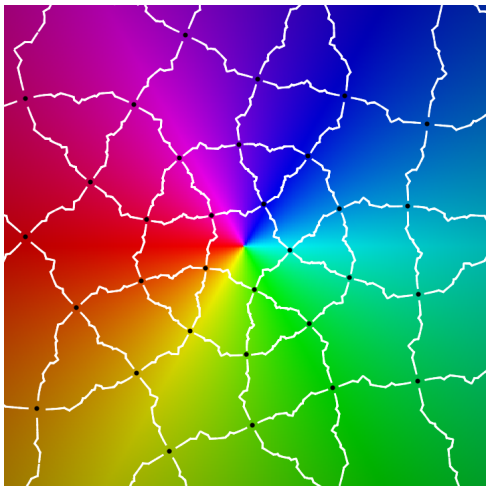

period 3

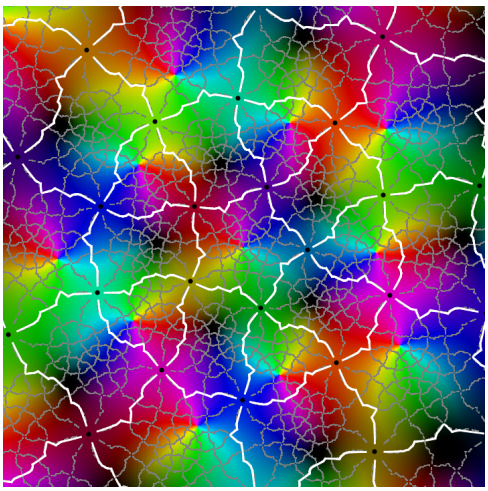

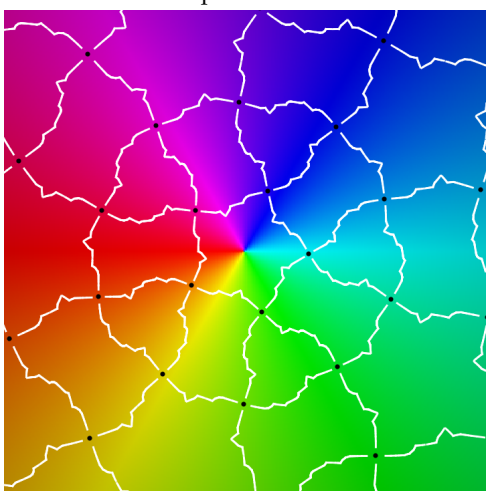

period 5

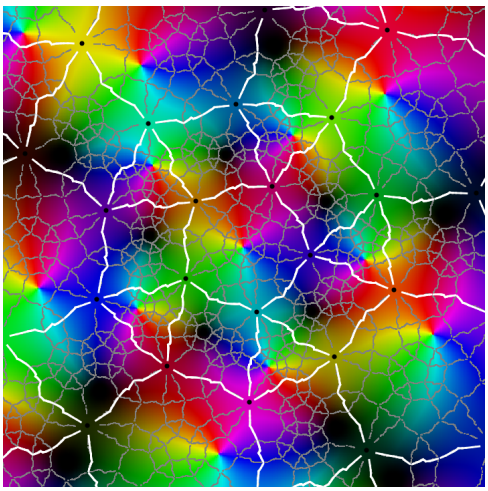

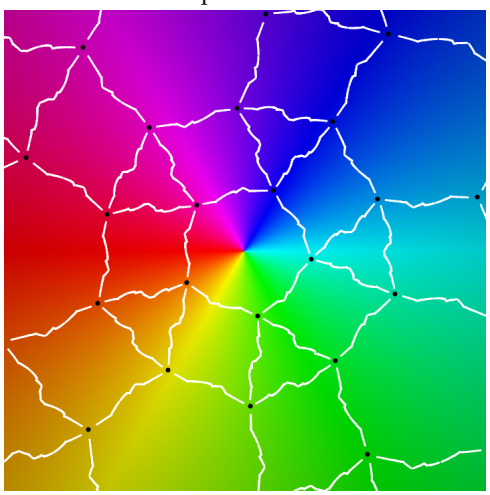

period 5

| | | $P$ | $T$ | $Q$ | $a \cdot X \longleftarrow$ total number of times $X$ faces are covered |
|---|---|---|---|---|---|
| $P$ | $\longrightarrow$ | 6 | 15 | 20 | $12 \cdot P \longleftarrow 12 \cdot 6 + 20 \cdot 3 + 30 \cdot 8 = 12 \cdot 31$ |
| $T$ | $\longrightarrow$ | 3 | 10 | 12 | $20 \cdot T \longleftarrow 12 \cdot 15 + 20 \cdot 10 + 30 \cdot 8 = 20 \cdot 31$ |
| $Q$ | $\longrightarrow$ | 8 | 8 | 15 | $30 \cdot Q \longleftarrow 12 \cdot 20 + 20 \cdot 12 + 30 \cdot 15 = 30 \cdot 31$ |

Peer-reviewed version available at Symmetry 2020, 12, 177; doi:10.3390/sym12010177



Class Ic

$$
\begin{aligned}
P &\longrightarrow \text{complement of six } P\text{-caps about } \widetilde{P} \\
T &\longrightarrow \text{complement of three } P\text{-caps about } \widetilde{T} \\
Q &\longrightarrow \text{four } P\text{-caps about } \widetilde{Q}
\end{aligned}
$$

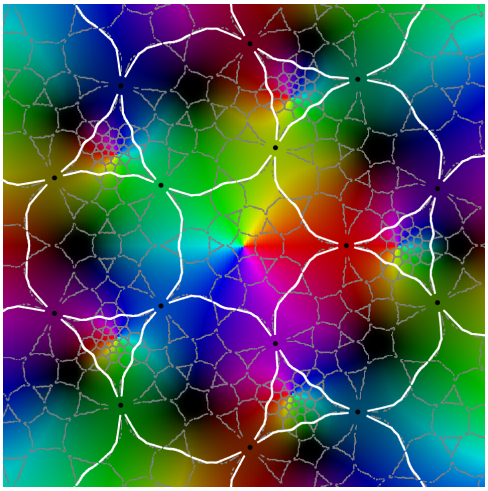

the map $h$ discussed in Section 6

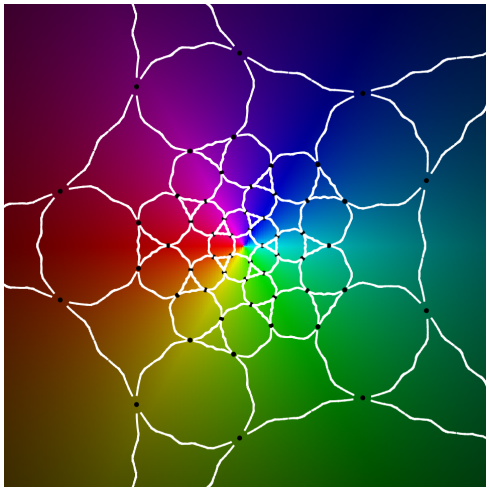

period 2, achiral

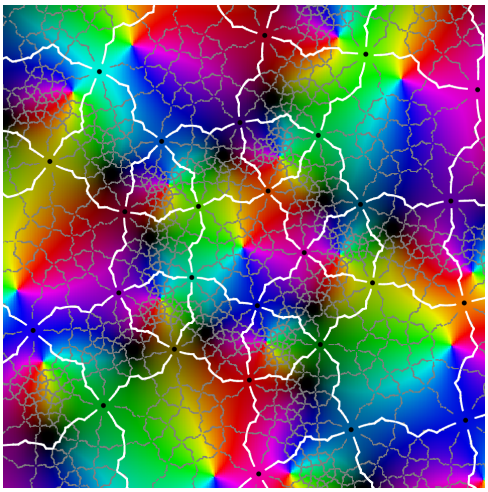

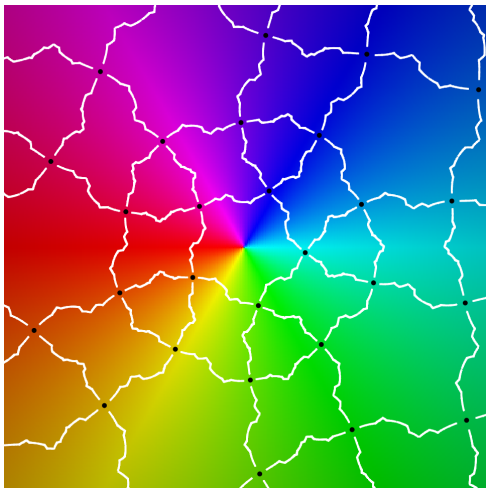

period 2

Peer-reviewed version available at Symmetry 2020, 12, 177; doi:10.3390/sym12010177



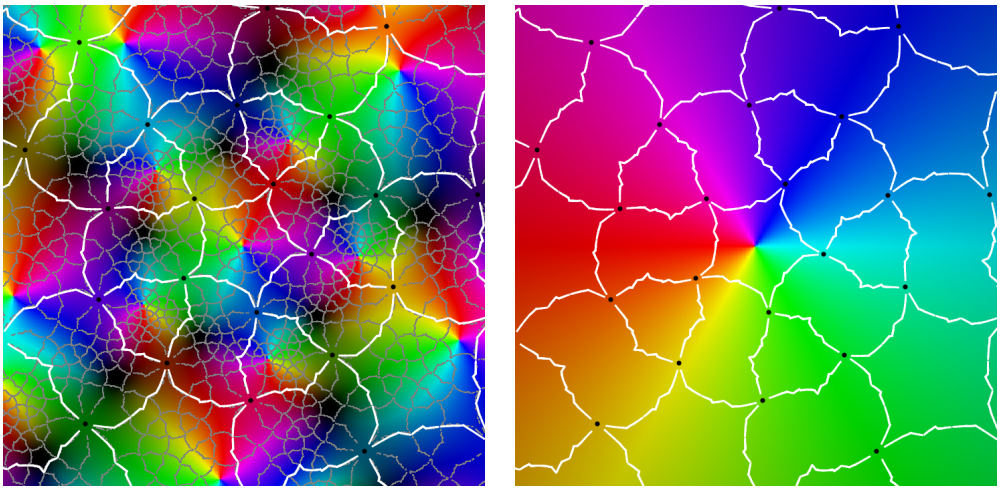

period 3

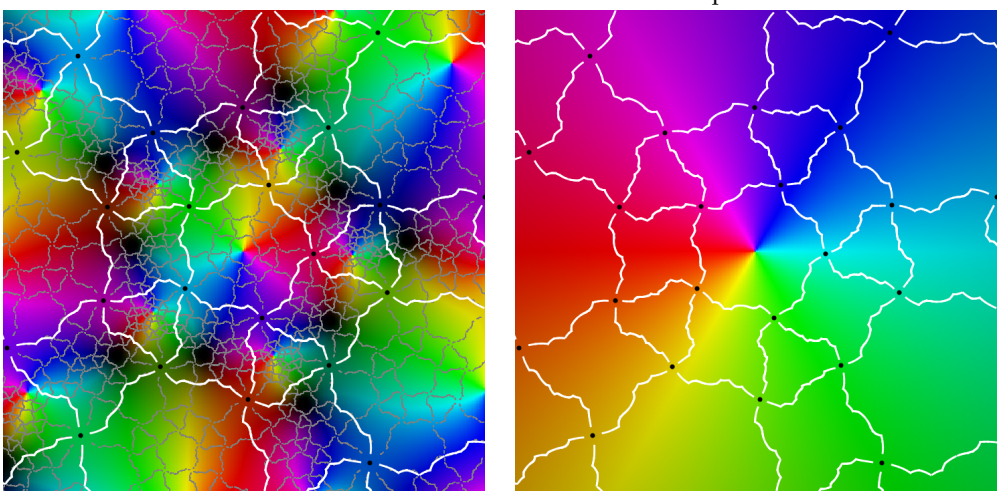

period 3

| | | $P$ | $T$ | $Q$ | $a \cdot X \longleftarrow$ total number of times $X$ faces are covered |
|---|---|---|---|---|---|
| $P$ | $\longrightarrow$ | 6 | 5 | 10 | $12 \cdot P \longleftarrow 12 \cdot 6 + 20 \cdot 9 + 30 \cdot 4 = 12 \cdot 31$ |
| $T$ | $\longrightarrow$ | 9 | 10 | 18 | $20 \cdot T \longleftarrow 12 \cdot 5 + 20 \cdot 10 + 30 \cdot 12 = 20 \cdot 31$ |
| $Q$ | $\longrightarrow$ | 4 | 12 | 15 | $30 \cdot Q \longleftarrow 12 \cdot 10 + 20 \cdot 18 + 30 \cdot 15 = 30 \cdot 31$ |

Peer-reviewed version available at Symmetry 2020, 12, 177; doi:10.3390/sym12010177



Class II

$P \longrightarrow$ one $P$-cap about $P$
$T \longrightarrow$ three $P$-caps about $T$
$Q \longrightarrow$ complement of two $P$-caps about $Q$

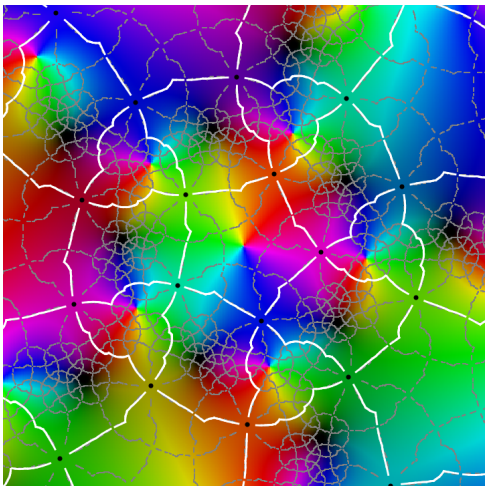

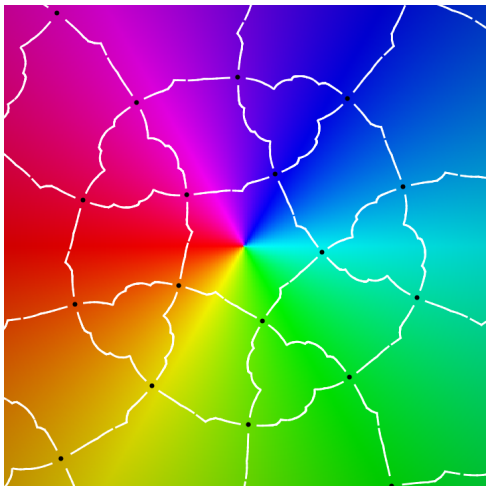

period 3

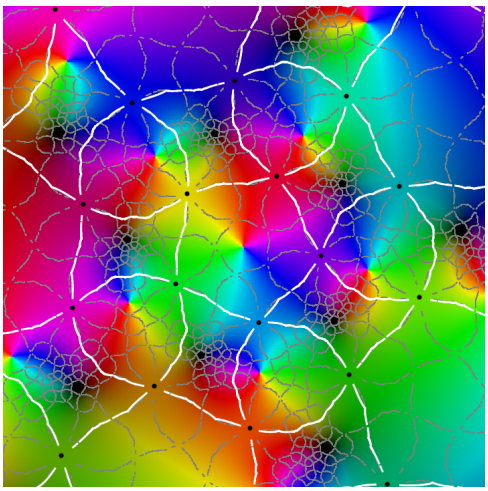

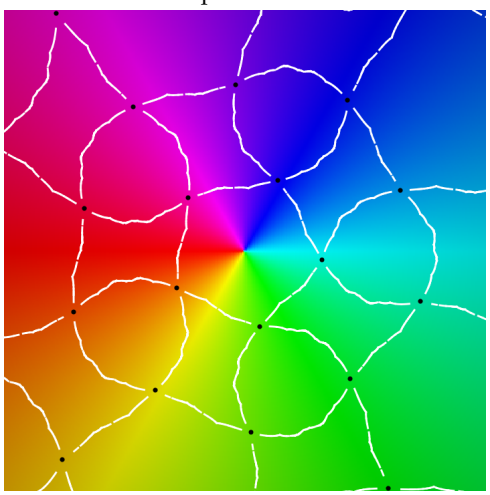

period 5

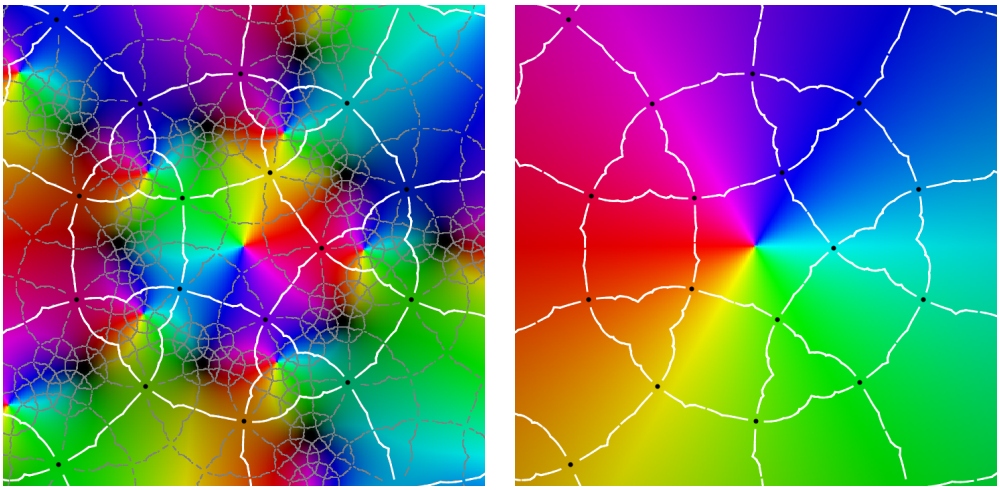

period 5

| | | $P$ | $T$ | $Q$ | $a \cdot X \longleftarrow$ total number of times $X$ faces are covered |
|---|---|---|---|---|---|
| $P$ | $\longrightarrow$ | 1 | 5 | 5 | $12 \cdot P \longleftarrow 12 \cdot 1 + 20 \cdot 3 + 30 \cdot 10 = 12 \cdot 31$ |
| $T$ | $\longrightarrow$ | 3 | 10 | 12 | $20 \cdot T \longleftarrow 12 \cdot 5 + 20 \cdot 10 + 30 \cdot 12 = 20 \cdot 31$ |
| $Q$ | $\longrightarrow$ | 10 | 12 | 21 | $30 \cdot Q \longleftarrow 12 \cdot 5 + 20 \cdot 12 + 30 \cdot 21 = 30 \cdot 31$ |

Peer-reviewed version available at Symmetry 2020, 12, 177; doi:10.3390/sym12010177



Class IIc

$P \longrightarrow$ complement of one $P$-cap about $\widetilde{P}$
$T \longrightarrow$ complement of three $P$-caps about $\widetilde{T}$
$Q \longrightarrow$ two $P$-caps about $\widetilde{Q}$

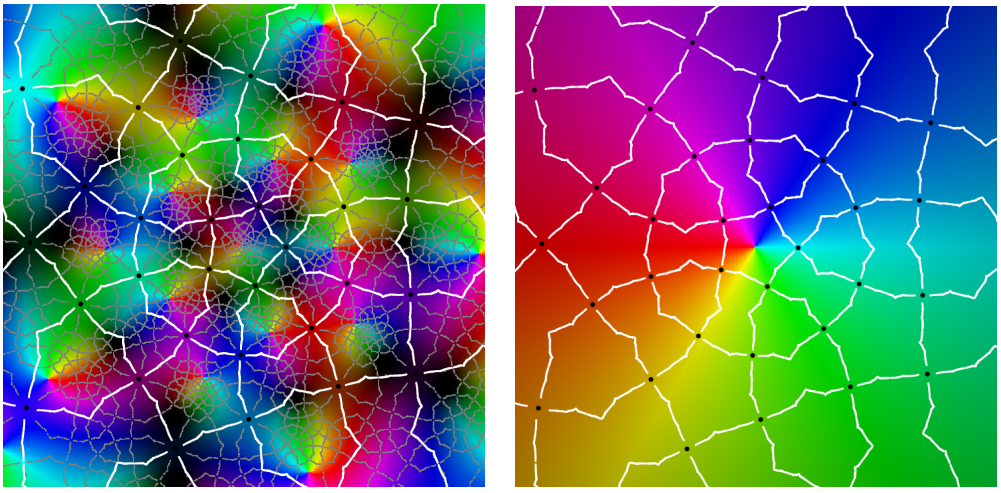

period 3

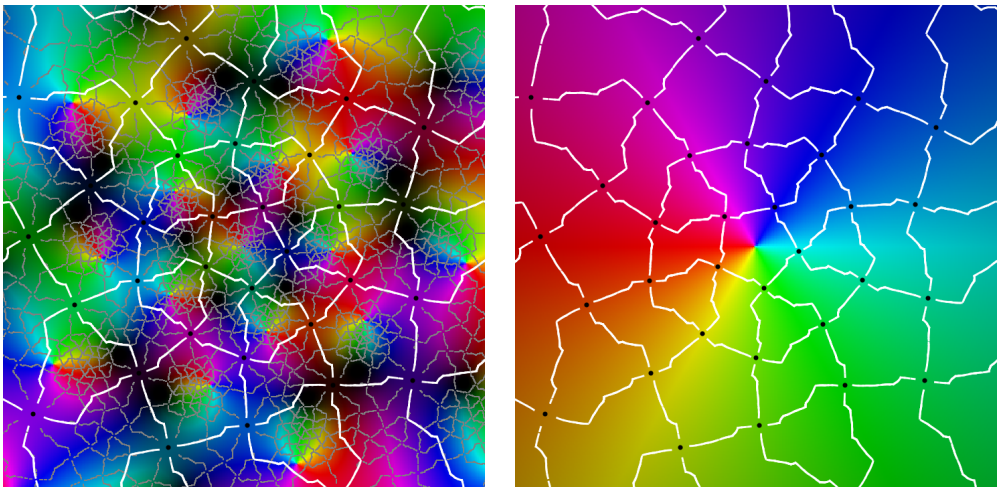

period 3

Peer-reviewed version available at *Symmetry* **2020**, *12*, 177; doi:10.3390/sym12010177



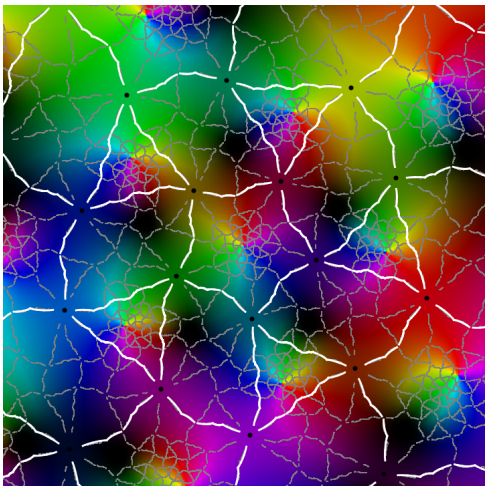

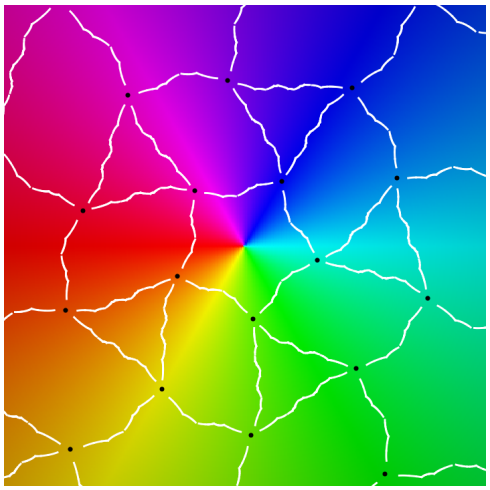

period 5

| | | $P$ | $T$ | $Q$ | $a \cdot X \longleftarrow$ total number of times $X$ faces are covered |
|---|---|---|---|---|---|
| $P$ | $\longrightarrow$ | 11 | 15 | 25 | $12 \cdot P \longleftarrow 12 \cdot 11 + 20 \cdot 9 + 30 \cdot 2 = 12 \cdot 31$ |
| $T$ | $\longrightarrow$ | 9 | 10 | 18 | $20 \cdot T \longleftarrow 12 \cdot 15 + 20 \cdot 10 + 30 \cdot 8 = 20 \cdot 31$ |
| $Q$ | $\longrightarrow$ | 2 | 8 | 9 | $30 \cdot Q \longleftarrow 12 \cdot 25 + 20 \cdot 18 + 30 \cdot 9 = 30 \cdot 31$ |

Peer-reviewed version available at Symmetry 2020, 12, 177; doi:10.3390/sym12010177



Class III

$P \longrightarrow$ six $P$-caps about $P$
$T \longrightarrow$ nine $P$-caps about $T$
$Q \longrightarrow$ complement of eight $P$-caps about $Q$

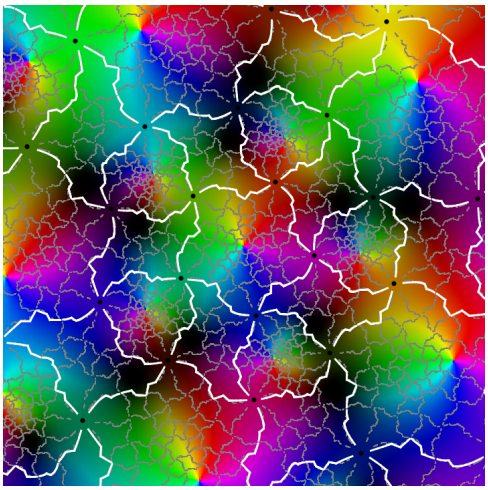

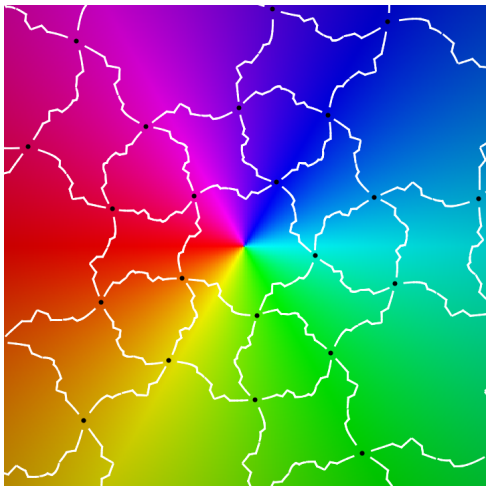

period 3

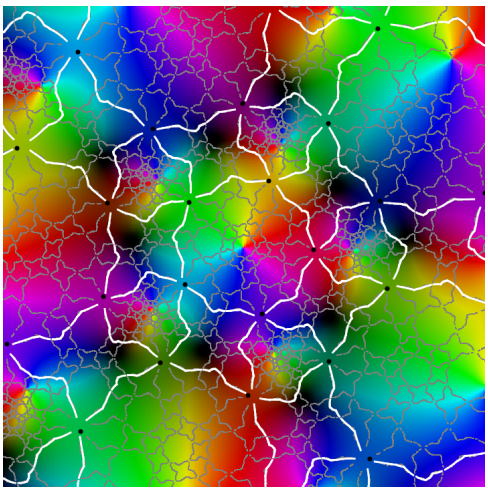

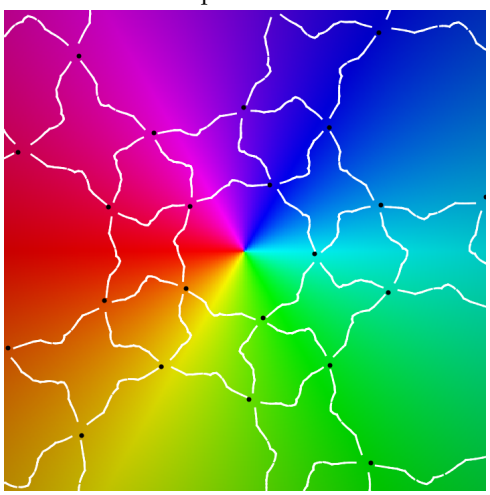

period 3

Peer-reviewed version available at Symmetry 2020, 12, 177; doi:10.3390/sym12010177



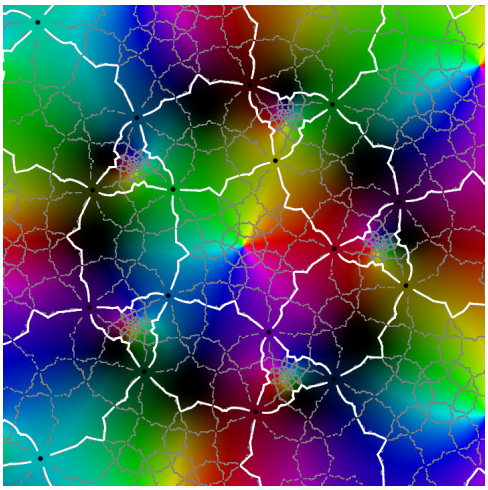

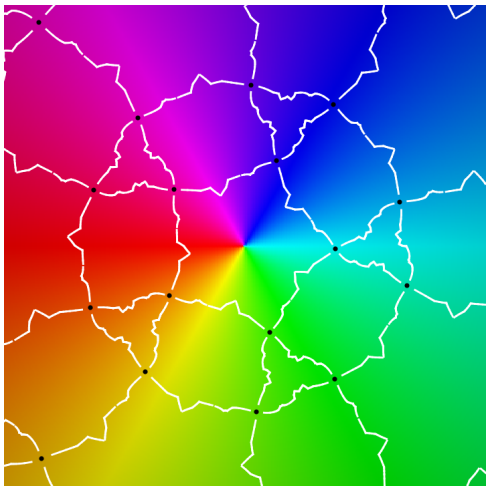

period 5

| | | $P$ | $T$ | $Q$ | $a \cdot X \longleftarrow$ total number of times $X$ faces are covered |
|---|---|---|---|---|---|
| $P$ | $\longrightarrow$ | 6 | 15 | 20 | $12 \cdot P \longleftarrow 12 \cdot 6 + 20 \cdot 9 + 30 \cdot 4 = 12 \cdot 31$ |
| $T$ | $\longrightarrow$ | 9 | 19 | 27 | $20 \cdot T \longleftarrow 12 \cdot 15 + 20 \cdot 19 + 30 \cdot 2 = 20 \cdot 31$ |
| $Q$ | $\longrightarrow$ | 4 | 2 | 5 | $30 \cdot Q \longleftarrow 12 \cdot 20 + 20 \cdot 27 + 30 \cdot 5 = 30 \cdot 31$ |

Peer-reviewed version available at Symmetry 2020, 12, 177; doi:10.3390/sym12010177



Class IIIc

$$
\begin{aligned}
P &\longrightarrow \text{complement of six } P\text{-cap about } \widetilde{P} \\
T &\longrightarrow \text{complement of nine } P\text{-caps about } \widetilde{T} \\
Q &\longrightarrow \text{eight } P\text{-caps about } \widetilde{Q}
\end{aligned}
$$

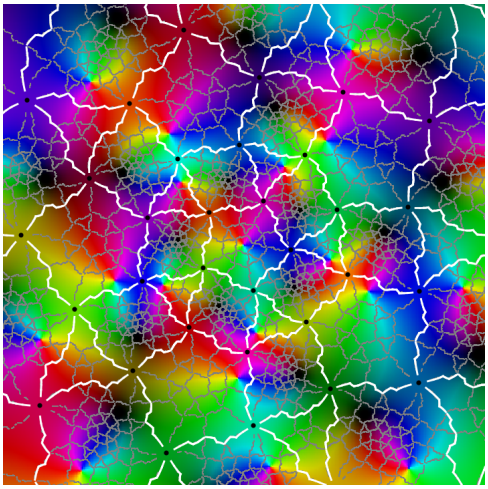

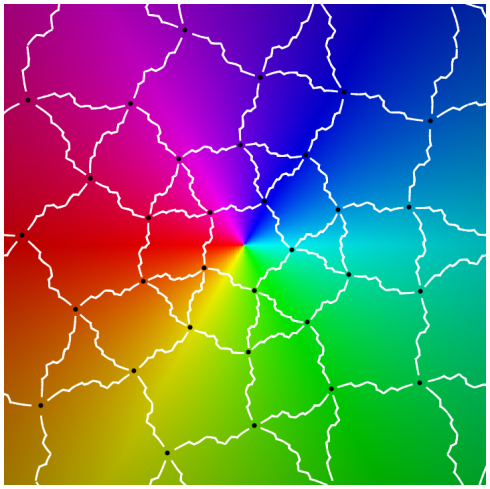

period 3

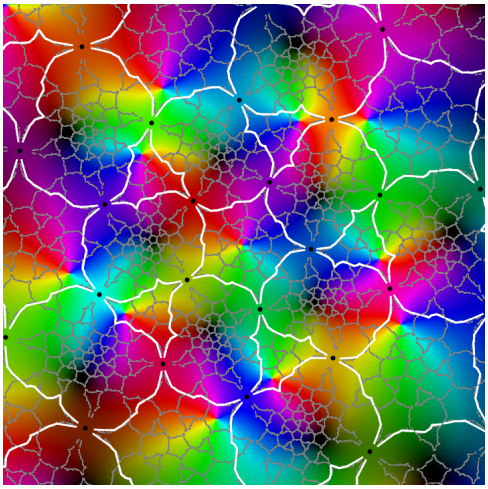

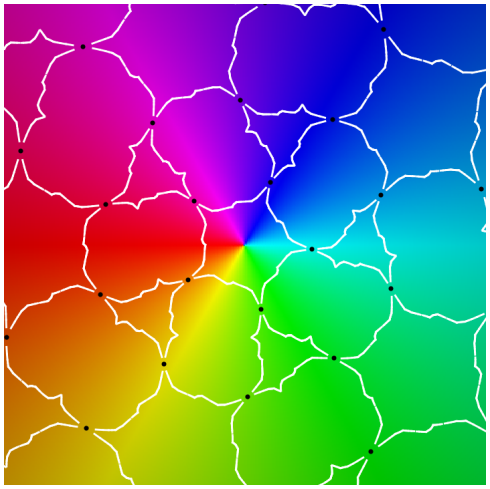

period 5

Peer-reviewed version available at Symmetry 2020, 12, 177; doi:10.3390/sym12010177



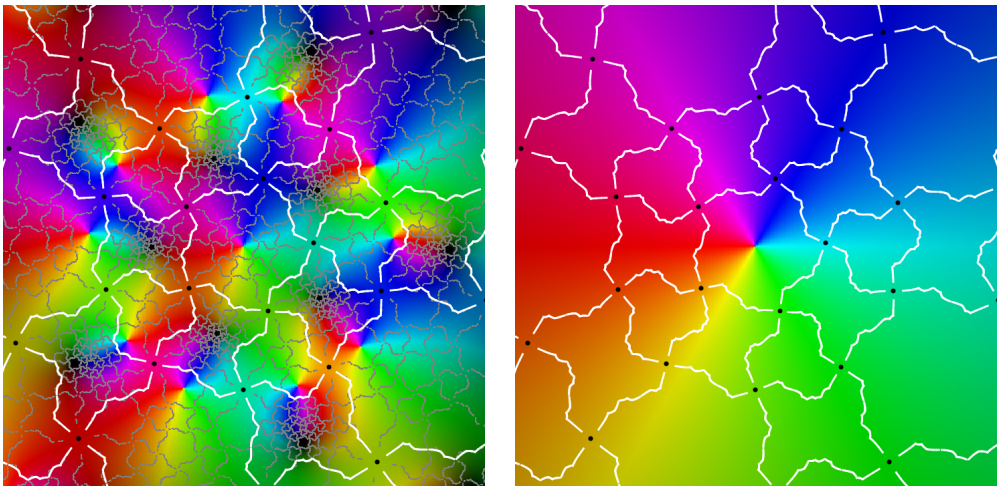

period 5

| | | $P$ | $T$ | $Q$ | $a \cdot X \longleftarrow$ total number of times $X$ faces are covered |
|---|---|---|---|---|---|
| $P$ | $\longrightarrow$ | 6 | 5 | 10 | $12 \cdot P \longleftarrow 12 \cdot 6 + 20 \cdot 3 + 30 \cdot 8 = 12 \cdot 31$ |
| $T$ | $\longrightarrow$ | 3 | 1 | 3 | $20 \cdot T \longleftarrow 12 \cdot 5 + 20 \cdot 1 + 30 \cdot 18 = 20 \cdot 31$ |
| $Q$ | $\longrightarrow$ | 8 | 18 | 25 | $30 \cdot Q \longleftarrow 12 \cdot 10 + 20 \cdot 3 + 30 \cdot 25 = 30 \cdot 31$ |

Peer-reviewed version available at Symmetry 2020, 12, 177; doi:10.3390/sym12010177



## Class IV

$$
\begin{aligned}
P &\longrightarrow P = \text{complement of 11 } P\text{-caps about } \widetilde{P} \\
T &\longrightarrow \text{complement of nine } P\text{-caps about } \widetilde{T} \\
Q &\longrightarrow \text{ten } P\text{-caps about } \widetilde{Q}
\end{aligned}
$$

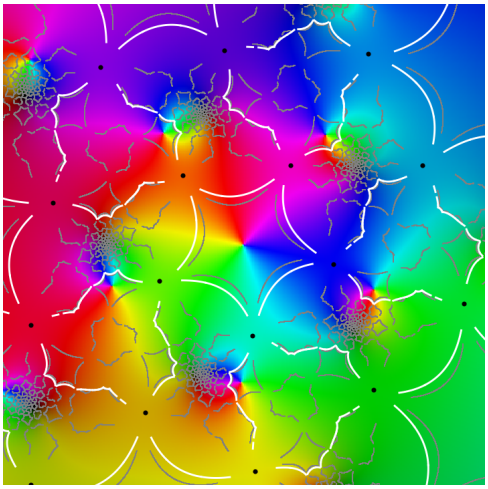

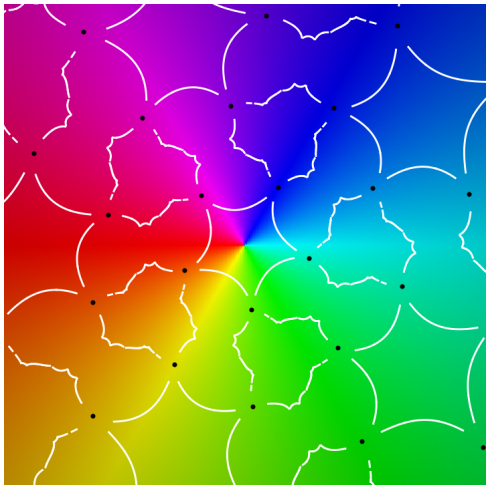

period 5

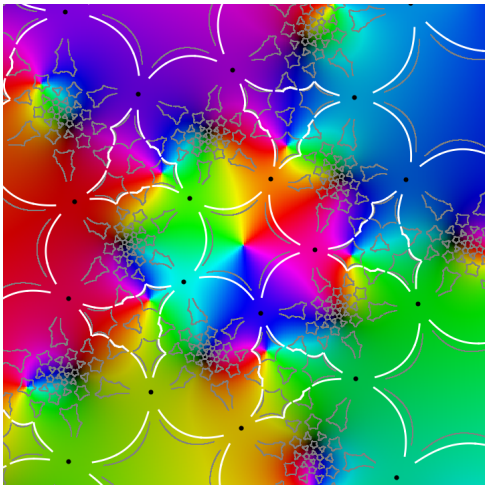

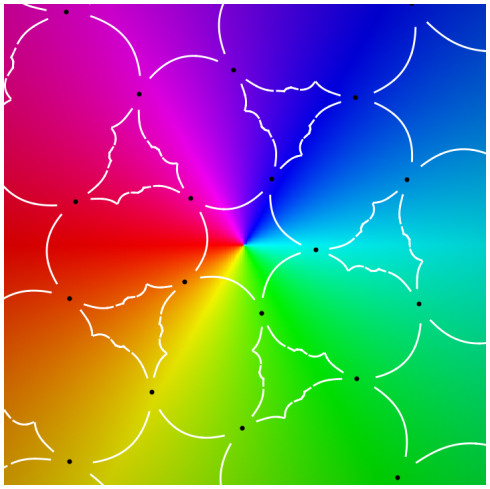

period 5

| | | $P$ | $T$ | $Q$ | $a \cdot X \longleftarrow$ total number of times $X$ faces are covered |
|---|---|---|---|---|---|
| $P$ | $\longrightarrow$ | 1 | 0 | 0 | $12 \cdot P \longleftarrow 12 \cdot 1 + 20 \cdot 3 + 30 \cdot 10 = 12 \cdot 31$ |
| $T$ | $\longrightarrow$ | 3 | 1 | 3 | $20 \cdot T \longleftarrow 12 \cdot 0 + 20 \cdot 1 + 30 \cdot 20 = 20 \cdot 31$ |
| $Q$ | $\longrightarrow$ | 10 | 20 | 29 | $30 \cdot Q \longleftarrow 12 \cdot 0 + 20 \cdot 3 + 30 \cdot 29 = 30 \cdot 31$ |

Peer-reviewed version available at Symmetry 2020, 12, 177; doi:10.3390/sym12010177



## Class IVc

$P \longrightarrow$ complement of $\widetilde{P} = 11$ $P$-caps about $P$
$T \longrightarrow$ nine $P$-caps about $T$
$Q \longrightarrow$ complement of ten $P$-caps about $Q$

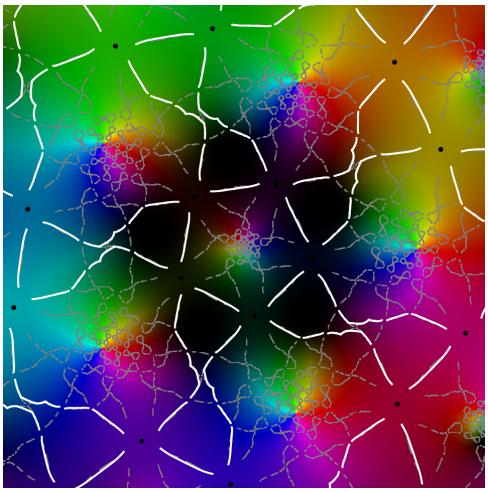

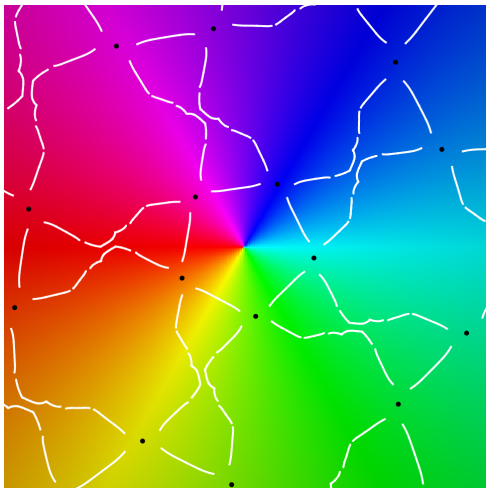

period 2

| | | $P$ | $T$ | $Q$ | $a \cdot X \longleftarrow$ total number of times $X$ faces are covered |
|---|---|---|---|---|---|
| $P$ | $\longrightarrow$ | 11 | 20 | 30 | $12 \cdot P \longleftarrow 12 \cdot 11 + 20 \cdot 9 + 30 \cdot 2 = 12 \cdot 31$ |
| $T$ | $\longrightarrow$ | 9 | 19 | 27 | $20 \cdot T \longleftarrow 12 \cdot 20 + 20 \cdot 19 + 30 \cdot 0 = 20 \cdot 31$ |
| $Q$ | $\longrightarrow$ | 2 | 0 | 1 | $30 \cdot Q \longleftarrow 12 \cdot 30 + 20 \cdot 27 + 30 \cdot 1 = 30 \cdot 31$ |

Peer-reviewed version available at Symmetry 2020, 12, 177; doi:10.3390/sym12010177



## Class V

$P \longrightarrow$ one $P$-cap about $P$

$T \longrightarrow$ complement of nine $P$-caps about $\widetilde{T}$

$Q \longrightarrow$ complement of 7-block about $Q$ (7-block $= Q$-cap $- 2 \cdot Q$)

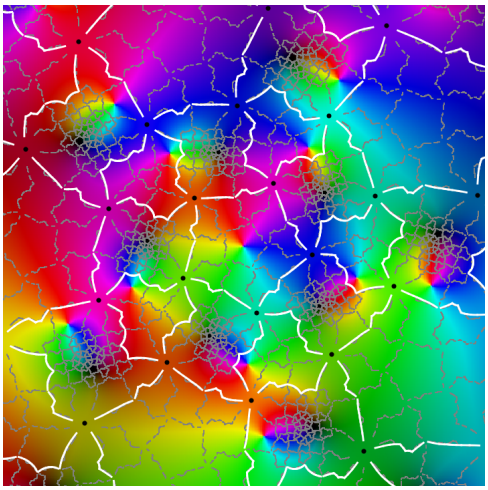

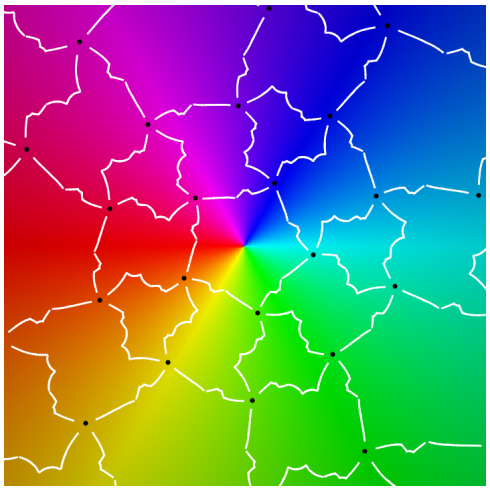

period 2

| | | $P$ | $T$ | $Q$ | $a \cdot X \longleftarrow$ total number of times $X$ faces are covered |
|---|---|---|---|---|---|
| $P$ | $\longrightarrow$ | 1 | 5 | 5 | $12 \cdot P \longleftarrow 12 \cdot 1 + 20 \cdot 3 + 30 \cdot 10 = 12 \cdot 31$ |
| $T$ | $\longrightarrow$ | 3 | 1 | 3 | $20 \cdot T \longleftarrow 12 \cdot 5 + 20 \cdot 1 + 30 \cdot 18 = 20 \cdot 31$ |
| $Q$ | $\longrightarrow$ | 10 | 18 | 27 | $30 \cdot Q \longleftarrow 12 \cdot 5 + 20 \cdot 3 + 30 \cdot 27 = 30 \cdot 31$ |

Peer-reviewed version available at Symmetry 2020, 12, 177; doi:10.3390/sym12010177



## Class Vc

$P \longrightarrow$ complement of one $P$-cap about $\widetilde{P}$

$T \longrightarrow$ nine $P$-caps about $T$

$Q \longrightarrow$ 7-block about $\widetilde{Q}$

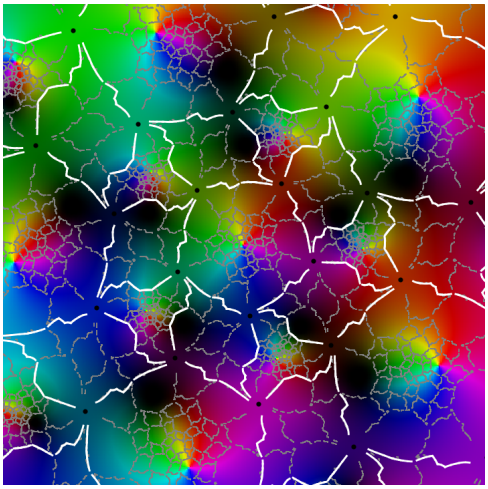

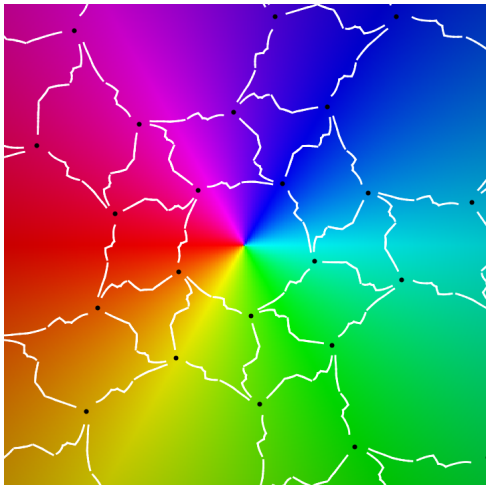

period 5

| | | $P$ | $T$ | $Q$ | $a \cdot X \longleftarrow$ total number of times $X$ faces are covered |
|---|---|---|---|---|---|
| $P$ | $\longrightarrow$ | 11 | 15 | 25 | $12 \cdot P \longleftarrow 12 \cdot 11 + 20 \cdot 9 + 30 \cdot 2 = 12 \cdot 31$ |
| $T$ | $\longrightarrow$ | 9 | 19 | 27 | $20 \cdot T \longleftarrow 12 \cdot 15 + 20 \cdot 19 + 30 \cdot 2 = 20 \cdot 31$ |
| $Q$ | $\longrightarrow$ | 2 | 2 | 3 | $30 \cdot Q \longleftarrow 12 \cdot 25 + 20 \cdot 27 + 30 \cdot 3 = 30 \cdot 31$ |

Peer-reviewed version available at Symmetry 2020, 12, 177; doi:10.3390/sym12010177



## Exceptional cases

$$P \longrightarrow \text{six } P\text{-caps about } P$$
$$T \longrightarrow \text{complement of three } P\text{-caps at } \widetilde{T}$$
$$Q \longrightarrow \text{two } P\text{-caps} \cup 2 \cdot P \cup 2 \cdot Q \text{ about } \widetilde{Q}$$

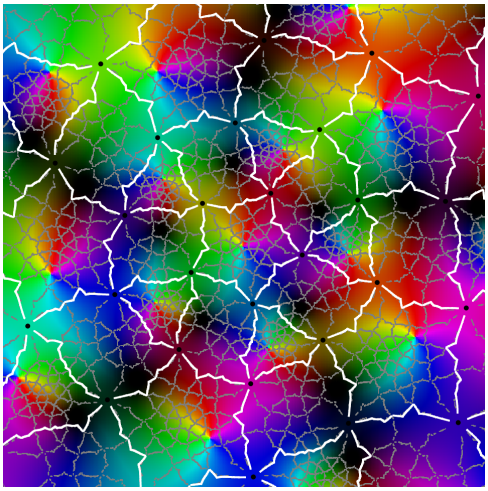

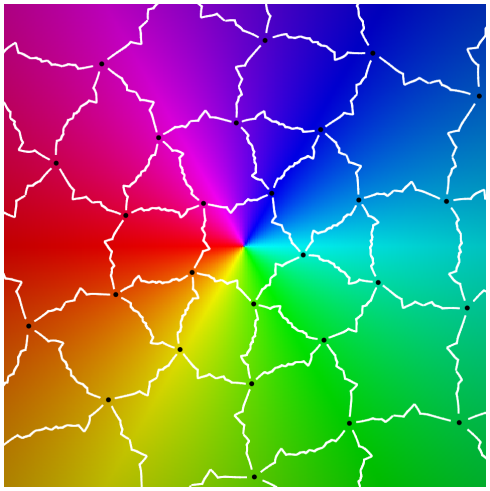

period 2

| | | $P$ | $T$ | $Q$ | $a \cdot X \longleftarrow$ total number of times $X$ faces are covered |
|---|---|---|---|---|---|
| $P$ | $\longrightarrow$ | 6 | 15 | 20 | $12 \cdot P \longleftarrow 12 \cdot 6 + 20 \cdot 9 + 30 \cdot 4 = 12 \cdot 31$ |
| $T$ | $\longrightarrow$ | 9 | 10 | 18 | $20 \cdot T \longleftarrow 12 \cdot 15 + 20 \cdot 10 + 30 \cdot 8 = 20 \cdot 31$ |
| $Q$ | $\longrightarrow$ | 4 | 8 | 11 | $30 \cdot Q \longleftarrow 12 \cdot 20 + 20 \cdot 18 + 30 \cdot 11 = 30 \cdot 31$ |

$$P \longrightarrow \text{one } P\text{-cap about } P$$
$$T \longrightarrow T$$
$$Q \longrightarrow 18\ T\text{-caps about } \widetilde{Q} \text{ (complement of } Q \cup 2 \cdot T)$$

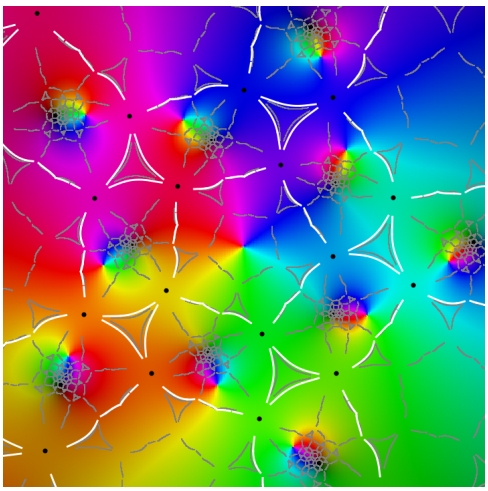

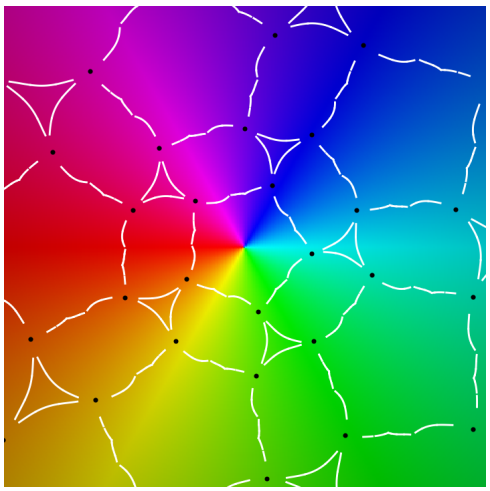

period 3

Peer-reviewed version available at Symmetry 2020, 12, 177; doi:10.3390/sym12010177



| | | $P$ | $T$ | $Q$ | $a \cdot X \longleftarrow$ total number of times $X$ faces are covered |
|---|---|---|---|---|---|
| $P$ | $\longrightarrow$ | 1 | 5 | 5 | $12 \cdot P \longleftarrow 12 \cdot 1 + 20 \cdot 0 + 30 \cdot 12 = 12 \cdot 31$ |
| $T$ | $\longrightarrow$ | 0 | 1 | 0 | $20 \cdot T \longleftarrow 12 \cdot 5 + 20 \cdot 1 + 30 \cdot 18 = 20 \cdot 31$ |
| $Q$ | $\longrightarrow$ | 12 | 18 | 29 | $30 \cdot Q \longleftarrow 12 \cdot 5 + 20 \cdot 0 + 30 \cdot 29 = 30 \cdot 31$ |

$P \longrightarrow$ complement of six $P$-caps about $\widetilde{P}$

$T \longrightarrow$ complement of six $P$-caps about $\widetilde{T}$

$Q \longrightarrow$ six $P$-caps about $\widetilde{Q}$

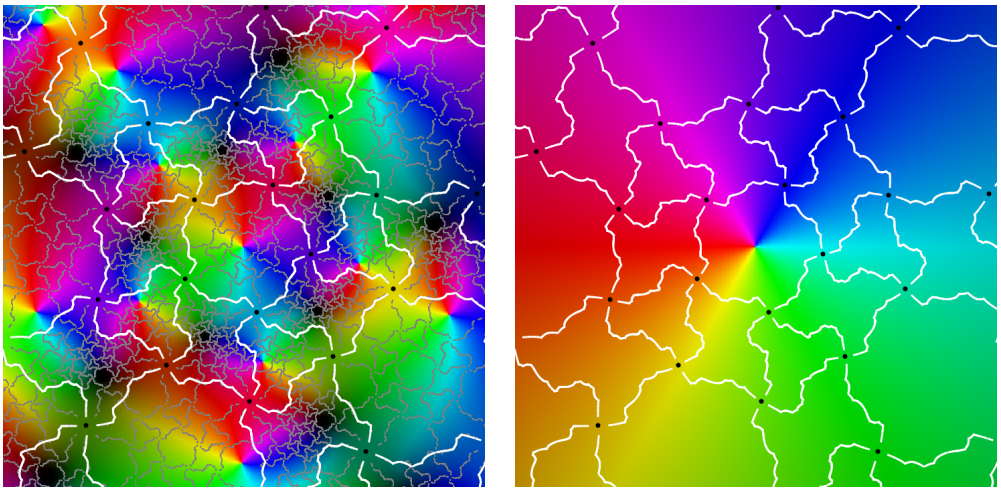

period 5

| | | $P$ | $T$ | $Q$ | $a \cdot X \longleftarrow$ total number of times $X$ faces are covered |
|---|---|---|---|---|---|
| $P$ | $\longrightarrow$ | 6 | 5 | 10 | $12 \cdot P \longleftarrow 12 \cdot 6 + 20 \cdot 6 + 30 \cdot 6 = 12 \cdot 31$ |
| $T$ | $\longrightarrow$ | 6 | 4 | 9 | $20 \cdot T \longleftarrow 12 \cdot 5 + 20 \cdot 4 + 30 \cdot 16 = 20 \cdot 31$ |
| $Q$ | $\longrightarrow$ | 6 | 16 | 21 | $30 \cdot Q \longleftarrow 12 \cdot 10 + 20 \cdot 9 + 30 \cdot 21 = 30 \cdot 31$ |

**Acknowledgments:** The work represented in this article grew out of discussions with Peter Doyle to whom I owe a large debt of gratitude.

B 1991. A. Beardon. *Iteration of Rational Functions*. Springer (1991)

C 2014. S. Crass. *Dynamics of a soccer ball*. Experiment. Math. 23 (2014) No. 3, 261-270.

C web. S. Crass. `www.csulb.edu/~scrass/math.html`

DH 1993. A. Douady and J. Hubbard. *A proof of Thurston's topological characterization of rational functions*. Acta Math. 171 (1993), No. 2, 263–297.

DM 1989. P. Doyle and C. McMullen. *Solving the quintic by iteration*. Acta Mathematica 163 (1989), 151-80.

K 1956. F. Klein. *Lectures on the icosahedron*. Dover Publ. (1956).

T 2016. D. Thurston. *A positive characterization of rational maps*. arXiv:1612.04424.